Quantum and semiclassical exceptional points of a linear system of coupled cavities with losses and gain within the Scully-Lamb laser theory

Ievgen I. Arkhipov, Adam Miranowicz, Fabrizio Minganti, and Franco Nori

Phys. Rev. A **101**, 013812 — Published 14 January 2020

DOI: 10.1103/PhysRevA.101.013812

Quantum and semiclassical exceptional points of a linear system of coupled cavities with losses and gain within the Scully-Lamb laser theory

Ievgen I. Arkhipov,[1,*] Adam Miranowicz,[2,3,†] Fabrizio Minganti,[3,‡] and Franco Nori[3,4,§]

[1] *Joint Laboratory of Optics of Palacký University and Institute of Physics of CAS, Faculty of Science, Palacký University, 17. listopadu 12, 771 46 Olomouc, Czech Republic*
[2] *Faculty of Physics, Adam Mickiewicz University, PL-61-614 Poznan, Poland*
[3] *Theoretical Quantum Physics Laboratory, RIKEN Cluster for Pioneering Research, Wako-shi, Saitama 351-0198, Japan*
[4] *Physics Department, The University of Michigan, Ann Arbor, Michigan 48109-1040, USA*

(Dated: November 26, 2019)

In the past few decades, many works have been devoted to the study of exceptional points (EPs), i.e., exotic degeneracies of non-Hermitian systems. The usual approach in those studies involves the introduction of a phenomenological effective non-Hermitian Hamiltonian (NHH), where the gain and losses are incorporated as the imaginary frequencies of fields, and from which the Hamiltonian EPs (HEPs) are derived. Although this approach can provide valid equations of motion for the fields in the classical limit, its application in the derivation of EPs in the quantum regime is questionable. Recently, a framework [Minganti *et al.*, arXiv:1909.11619], which allows to determine quantum EPs from a Liouvillian (LEPs), rather than from an NHH, has been proposed. Compared to the NHHs, a Liouvillian naturally includes quantum noise effects via quantum-jump terms, thus, allowing to consistently determine its EPs purely in the quantum regime. In this work, we study a non-Hermitian system consisting of coupled cavities with unbalanced gain and losses, and where the gain is far from saturation, i.e, the system is assumed to be linear. We apply both formalisms, based on an NHH and a Liouvillian within the Scully-Lamb laser theory, to determine and compare the corresponding HEPs and LEPs in the semiclassical and quantum regimes. ♣ Our results indicate that, although the overall spectral properties of the NHH and the corresponding Liouvillian for a given system can differ substantially, their LEPs and HEPs occur for the same combination of system parameters.

I. INTRODUCTION

Non-Hermiticity plays a crucial role in the studies of the dynamics of quantum systems. Non-Hermiticity refers to the systems described by Hamiltonians that are non-Hermitian, i.e., the energy spectra are represented by complex values. The positive or negative imaginary parts of the eigenvalues of a non-Hermitian Hamiltonian (NHH) indicate that a given system undergoes either amplification or dissipation processes, respectively. The best known examples of non-Hermitian systems are open quantum systems, where a quantum system of interest interacts with an environment, where the latter induces decoherence of the former.

Recently, a new surge of interest in non-Hermitian systems has been triggered by the discovery of a class of non-Hermitian Hamiltonians, which commute with a parity-time ($\mathcal{PT}$) operator, with real eigenvalues [1].

Initially, $\mathcal{PT}$-symmetric systems were merely an object of mathematical interest, as there was a little understanding on how to implement such systems in practice. It was only later realized that $\mathcal{PT}$-symmetry can be carried out in photonics, thanks to the analogy of the Schrödinger equation in quantum mechanics and the paraxial Maxwell equation in classical physics [2–6]. In the latter case, this analogy can be explored by making the profile of the real and imaginary parts of the optical index of a medium symmetric and asymmetric, respectively. Thus, one can obtain the system, which exhibits a $\mathcal{PT}$ symmetry-like behavior, by properly balancing gain and losses of the system.

One of the most peculiar properties of non-Hermitian systems, in particular those which are $\mathcal{PT}$-symmetric, is the presence of the so-called exceptional points (EPs), i.e., system degeneracies, where both eigenvalues and their corresponding eigenvectors of an NHH coincide. The behavior of physical systems near EPs can lead to the observation of nontrivial phenomena in photonics [2, 3]. These include: unidirectional invisibility [7, 8], lasers with and enhanced-mode selectivity [9, 10], low-power nonreciprocal light transmission [11, 12], thresholdless phonon lasers [13, 14], enhanced light-matter interactions [15–17], loss-induced lasing [18, 19]. EPs have been discussed in electronics [20], optomechanics [13, 21, 22], acoustics [23, 24], plasmonics [25], and metamaterials [26]. The concept of EPs has been successfully applied in the description of dynamical quantum phase transitions and topological phases of matter in open quantum systems (see, e.g., [27–36]).

So far, the concept of EPs in photonics has been mostly exploited within the framework of effective NHHs, where gain and losses are introduced phenomenologically into the Hamiltonians as the imaginary part of the field frequencies. The use of such an approach can be justified in the semiclassical regime, i.e., when considering intense classical fields. However, that approach can fail

* ievgen.arkhipov@upol.cz
† miran@amu.edu.pl
‡ fabrizio.minganti@riken.jp
§ fnori@riken.jp

in the quantum regime, where the explicit inclusion of quantum noise and spontaneous emission becomes necessary. Needless to say, quantum noise leads to symmetry breaking, in particular, $\mathcal{PT}$-symmetry breaking [37]. The quantum noise in a system can be precisely simulated by either the master equation (ME) [38, 39] or the quantum trajectory method [40, 41]. Of course, one can also resort to quantum Langevin forces within the framework of an NHH, but such an approach bears a phenomenological character, and, in some cases, can lead to erroneous results [38, 42].

The ME with a Liouvillian superoperator captures all the dynamics of an open quantum system with Markovian gain and losses. Recently, the concept of EPs based on the degeneracies of the Liouvillian rather than of an effective NHH has been introduced in Refs. [43, 44]. The study of the spectrum of a Liouvillian provides a framework for the investigation of the properties of non-Hermitian systems and their EPs in a rigorous quantum approach [44–50].

In this work, we focus on a *linear* non-Hermitian system consisting of two coupled active and passive cavities with gain and loss, respectively. The system is assumed to be linear, because the active cavity is assumed to operate far below the lasing threshold.

We study and compare EPs derived from two different formalisms based on an effective NHH and a Liouvillian. The Hamiltonian EPs are denoted as HEPs, and those derived from a Liouvillian are denoted as LEPs, correspondingly. Furthermore, we analyze HEPs and LEPs in both semiclassical (i.e., when quantum jumps can be effectively ignored, which usually is the case for systems with large mean photon number, $\langle\hat{n}\rangle \gg 1$) and quantum regimes (i.e., when quantum jumps cannot be ignored, e.g., for quantum systems with very small mean photon number $\langle\hat{n}\rangle \ll 1$). In both regimes, we treat the fields as q-numbers.

In the semiclassical regime, we determine HEPs from the eigenspectra of the Hamiltonian, which is written in a finite-matrix form, whereas LEPs are derived via a two-time correlation function (TTCF), since a direct diagonalization of the Liouvillian is almost impossible for $\langle\hat{n}\rangle \gg 1$. On the contrary, in the quantum single-photon limit, both Hamiltonian and Liouvillian can be represented as finite matrices; thus, allowing us to determine their HEPs and LEPs solely from their eigenspectra.

Our results indicate that the same combination of system parameters leads to the occurrence of HEPs and LEPs in either regime. Remarkably, the overall spectral properties of the Liouvillian and NHH can differ substantially. ♣ Indeed, we find that LEPs can be of higher order than that of the corresponding HEPs.

Additionally, when considering the semiclassical regime, we provide a comparison of LEPs determined from both TTCFs and spectral bifurcation points (SBPs) of power spectra. Thus, we present a comparison of LEPs defined in two complementary domains. This comparison reveals that, in general, only TTCFs can be used for identifying a true LEP in the semiclassical limit.

Full name	Abbreviation
Non-Hermitian Hamiltonian	NHH
Exceptional point	EP
Hamiltonian exceptional point (an EP of an NHH)	HEP
Liouvillian exceptional point (an EP of a Liouvillian)	LEP
Spectral bifurcation point (a bifurcation point of a power spectrum)	SBP
Master equation	ME
Two-time correlation function	TTCF

TABLE I. Abbreviations used in this paper.

The paper is organized as follows. In Sec. II, we introduce both Liouvillian and effective NHH for the linear system of coupled active and passive cavities. In Secs. III and IV, we study and compare HEPs and LEPs in the semiclassical and quantum regimes, respectively. Conclusions are drawn in Sec. V.

Through the text of this paper we deal with several abbreviations. Therefore, in order to avoid any confusion when encountering them, we list all of them in Table I.

II. GENERAL THEORY OF THE SCULLY-LAMB MODEL IN THE QUANTUM LIMIT

The object of our study is the system of two coupled cavities, sketched in Fig. 1, where one cavity is active, i.e., it can provide gain for fields, and another cavity is passive, i.e., it induces only losses. Additionally, each resonator is coupled to a waveguide (see Fig. 1).

The Hamiltonian of the system can be written as follows

$$\hat{H} = \sum_{k=1}^{2} \hbar\omega_k \hat{a}_k^\dagger \hat{a}_k + i\hbar\kappa(\hat{a}_1\hat{a}_2^\dagger - \text{H.c.}), \tag{1}$$

where $\hat{a}_k$ ($\hat{a}_k^\dagger$) is the boson annihilation (creation) operator of the mode $k = 1, 2$, with frequency ω_k; and H.c. denotes Hermitian conjugate. Moreover, κ is the real coupling strength between the resonators.

To incorporate loss and gain in the cavities on the quantum level, one can resort to the Scully-Lamb ME [38, 51], which has the following form

$$\begin{aligned}\frac{d}{dt}\hat{\rho} = \frac{1}{i\hbar}\left[\hat{H}, \hat{\rho}\right] + \Big[&\frac{A}{2}(\hat{a}_1^\dagger\hat{\rho}\hat{a}_1 - \hat{a}_1\hat{a}_1^\dagger\hat{\rho}) \\ &+ \frac{B}{8}\Big(\hat{\rho}(\hat{a}_1\hat{a}_1^\dagger)^2 + 3\hat{a}_1\hat{a}_1^\dagger\hat{\rho}\hat{a}_1\hat{a}_1^\dagger - 4\hat{a}_1^\dagger\hat{\rho}\hat{a}_1\hat{a}_1^\dagger\hat{a}_1\Big) \\ &+ \sum_{i=1}^{2}\frac{\Gamma_i}{2}(\hat{a}_i\hat{\rho}\hat{a}_i^\dagger - \hat{a}_i^\dagger\hat{a}_i\hat{\rho}) + \text{H.c.}\Big],\end{aligned} \tag{2}$$

given in terms of the gain A and gain saturation B coefficients for the field in the active cavity. This equation

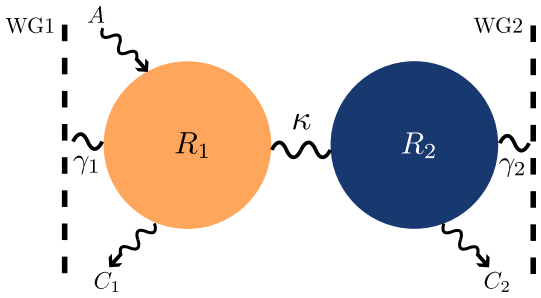

FIG. 1. ♣ Setup of the system of linearly coupled active and passive resonators. The active cavity R_1 has a gain rate A and the total loss rate $\Gamma_1 = C_1+\gamma_1$, consisting of the intrinsic loss rate C_1 and the loss rate γ_1 due to the coupling of R_1 to the waveguide WG1. The passive cavity R_2 has a total leakage rate $\Gamma_2 = C_2 + \gamma_2$, with C_2 and γ_2 being an intrinsic loss and a leakage loss to the waveguide WG2, respectively. The coupling strength between the active R_1 and passive R_2 resonators is denoted as κ.

describes the dynamics of the photonic part of a quantum laser, and, accordingly, the coefficients can be expressed as:

$$A = \frac{2g^2 r}{Y^2}, \quad \text{and} \quad B = \frac{4g^2}{Y^2}A, \tag{3}$$

where the parameter g stands for the coupling strength between the atoms of the gain medium and the optical field in the active cavity, Y is the decay rate of the atoms, and r accounts for the pump rate of the gain medium. In Eq. (2), the total decay rates for both cavities are given by ($i = 1, 2$)

$$\Gamma_i = C_i + \gamma_i, \tag{4}$$

where C_i is the intrinsic loss of the ith cavity, and γ_i stands for the loss due to the possible coupling of the ith cavity to the ith waveguide.

A. Liouvillian and effective non-Hermitian Hamiltonian for the system of coupled active and passive cavities in the weak-gain-saturation regime

The ME, given in Eq. (2), can be recast to the equation with a Lindblad Liouvillian superoperator $\mathcal{L}$ as follows [41]:

$$\begin{aligned}\frac{d}{dt}\hat{\rho} &= \mathcal{L}\hat{\rho}(t) \\ &= \frac{1}{i\hbar}\left[\hat{H},\hat{\rho}\right] - \frac{1}{2}\sum_{i=1}^{4}\left(\hat{L}_i^\dagger\hat{L}_i\hat{\rho} + \hat{\rho}\hat{L}_i^\dagger\hat{L}_i - 2\hat{L}_i\hat{\rho}\hat{L}_i^\dagger\right),\end{aligned} \tag{5}$$

where the Lindblad operators $\hat{L}_i$ (for $i = 1, \ldots, 4$) are defined as:

$$\begin{aligned}\hat{L}_1 = \sqrt{A}\hat{a}_1^\dagger\left(1 - \tfrac{B}{2A}\hat{a}_1\hat{a}_1^\dagger\right), \quad \hat{L}_2 = \tfrac{1}{2}\sqrt{3B}\hat{a}_1\hat{a}_1^\dagger, \\ \hat{L}_3 = \sqrt{\Gamma_1}\hat{a}_1, \quad \hat{L}_4 = \sqrt{\Gamma_2}\hat{a}_2.\end{aligned} \tag{6}$$

The Lindblad form in Eq. (5) is equivalent to the ME in Eq. (2) if the terms of second order in $B\hat{a}_1\hat{a}_1^\dagger/(2A)$ are neglected in Eq. (5), which holds true for the weak-gain-saturation regime.

When the active cavity is far below the lasing threshold and it is not driven by an intense coherent field, the gain saturation parameter B can be safely dropped, and the ME in Eq. (5) reduces to the following ME with a linear gain:

$$\begin{aligned}\frac{d}{dt}\hat{\rho} = \mathcal{L}\hat{\rho}(t) = \frac{1}{i\hbar}\left[\hat{H},\hat{\rho}\right] + \frac{A}{2}(2\hat{a}_1^\dagger\hat{\rho}\hat{a}_1 - \hat{a}_1\hat{a}_1^\dagger\hat{\rho} - \hat{\rho}\hat{a}_1\hat{a}_1^\dagger) \\ + \sum_{i=1}^{2}\frac{\Gamma_i}{2}(2\hat{a}_i\hat{\rho}\hat{a}_i^\dagger - \hat{a}_i^\dagger\hat{a}_i\hat{\rho} - \hat{\rho}\hat{a}_i^\dagger\hat{a}_i).\end{aligned} \tag{7}$$

From now on, we will always assume that the system of the coupled active and passive cavities is linear. Thus, we only consider the linear ME given in Eq. (7). The ME, in Eq. (7), as well as in Eq. (2), incorporates both quantum jump term $\hat{O}\hat{\rho}\hat{O}^\dagger$, and the continuous amplification or dissipation terms $\hat{O}\hat{O}^\dagger\hat{\rho} + \hat{\rho}\hat{O}\hat{O}^\dagger$.

We notice that the Liouvillian in Eq. (7) is quite general, and is *not* only limited to the description of quantum lasers in the linear-gain approximation. Indeed, Eq. (7) describes also an incoherently driven bosonic dimer. Recently, several incoherent driving mechanisms have been proposed [52–54], and the presence of photon-photon interaction was shown to induce a critical behavior in lattices of resonators [55, 56]. Since LEPs suggest the presence of a dissipative phase transition [45] and can occur also far from the thermodynamic limit, the study of the EPs in the dimer model relates to criticality and spontaneous-symmetry breaking characterizing the phase transition of the full lattice model.

On the other hand, in the vast literature devoted to $\mathcal{PT}$-symmetric systems with balanced gain and losses, one can often encounter the use of the following phenomenological *effective* NHH:

$$\hat{H}_{\text{eff}} = \hat{H} + \frac{i\hbar}{2}A\hat{a}_1^\dagger\hat{a}_1 - \frac{i\hbar}{2}\sum_{j=1}^{2}\Gamma_j\hat{a}_j^\dagger\hat{a}_j, \tag{8}$$

where the unitary Hamiltonian $\hat{H}$ is given in Eq. (1). As one can see, this NHH incorporates the gain and losses rates as the imaginary part of the field frequencies.

The NHH $\hat{H}_{\text{eff}}$, in Eq. (8), gives the same dynamics for the fields $\hat{a}_j$, $j = 1, 2$, as the ME in Eq. (7), but fails to explicitly incorporate quantum noise; thus, making the NHH usable, in general, only in the semiclassical limit. The detailed discussion of the actual semiclassical limit in this model will be in Sec. III.

Below, we calculate the HEPs and LEPs of the NHH $\hat{H}_{\text{eff}}$ in Eq. (8) and Liouvillian $\mathcal{L}$ in Eq. (7), respectively, in both semiclassical and quantum regimes for a given linear system in order to reveal their differences.

B. Liouvillian spectrum and exceptional points

Before we analyze the EPs of the Scully-Lamb model, let us first briefly recall some key properties of the Liouvillian spectrum [43, 45].

1. *Diagonalization of the Liouvillian superoperator*

The spectrum of the Liouvillian $\mathcal{L}$, given in Eq. (7), is found according to the formula

$$\mathcal{L}\hat{\rho}_i = \lambda_i \hat{\rho}_i, \tag{9}$$

where λ_i and $\hat{\rho}_i$ are the eigenvalues and eigenmatrices of the Liouvillian, respectively. We can always order the eigenvalues and eigenmatrices in such a way that $\mathrm{Re}[\lambda_0] < \mathrm{Re}[\lambda_1] \leq \mathrm{Re}[\lambda_2] \ldots$. Moreover, since the superoperator $\mathcal{L}$ is not necessarily Hermitian, it can acquire both right ($\mathcal{L}\hat{\rho}_i = \lambda\hat{\rho}_i$) and left ($\mathcal{L}^\dagger\hat{\sigma}_i = \lambda_i^*\hat{\sigma}_i$) eigenmatrices, respectively. The left and right eigenmatrices obey the following relation $\mathrm{Tr}[\hat{\rho}_i\hat{\sigma}_j] = \delta_{ij}$. If $\mathcal{L}$ is diagonalizable, the density matrix $\hat{\rho}(t)$ of the system can be written as follows

$$\hat{\rho}(t) = \sum_i c_i(t)\hat{\rho}_i, \tag{10}$$

where $c_i(t) = \exp(\lambda_i t)\,\mathrm{Tr}[\hat{\sigma}_i\hat{\rho}(0)]$.

The eigenvalue $\lambda_0 = 0$ of the Liouvillian $\mathcal{L}$ in Eq. (9) defines the steady-state density matrix $\hat{\rho}_{\mathrm{ss}} \propto \hat{\rho}_0$ of the system. The proportionality factor depends on the normalisation choice which is done on $\hat{\rho}_0$. Indeed, one often induces the standard Hilbert-Schmidt norm, so that $\|\hat{\rho}_0\|^2 = \mathrm{Tr}\left[\hat{\rho}_0^\dagger\hat{\rho}_0\right] = 1$, while instead $\mathrm{Tr}\left[\hat{\rho}_{\mathrm{ss}}\right] = 1$. For the remaining nonzero eigenvalues $\lambda_i \neq 0$ the corresponding eigenmatrices $\hat{\rho}_i$ are traceless, i.e., $\mathrm{Tr}[\hat{\rho}_i] = 0$.

If $\lambda_i \in \mathbb{R}$, then the corresponding eigenmatrix $\hat{\rho}_i$ is Hermitian. In this case, by diagonalizing the eigenmatrix

$$\rho_i = \sum_n p_n^{(i)} |\psi_n^{(i)}\rangle\langle\psi_n^{(i)}|, \tag{11}$$

one can consider the following decomposition $\hat{\rho}_i = \hat{\rho}_i^+ - \hat{\rho}_i^-$, where

$$\hat{\rho}_i^+ = \sum_{n\leq\bar{n}} p_n^{(i)} |\psi_n^{(i)}\rangle\langle\psi_n^{(i)}|, \quad \text{with} \quad p_n^{(i)} \geq 0, \tag{12}$$

and

$$\hat{\rho}_i^- = -\sum_{n>\bar{n}} p_n^{(i)} |\psi_n^{(i)}\rangle\langle\psi_n^{(i)}|, \quad \text{with} \quad p_n^{(i)} < 0, \tag{13}$$

and such that $\mathrm{Tr}[\hat{\rho}_i^+] = \mathrm{Tr}[\hat{\rho}_i^-] = 1$. The latter stems from the fact that the eigenmatrix $\hat{\rho}_i$ is traceless and one can always rearrange the coefficients $p_n^{(i)}$ such that $p_n^{(i)} > 0$ when $n \leq \bar{n}$, and $p_n^{(i)} < 0$ when $n > \bar{n}$. Now with such a decomposition, the wave-functions constituting both $\hat{\rho}_i^\pm$ can be compared with those comprising the corresponding effective NHH.

When $\lambda_i \in \mathbb{C}$, the eigenmatrix $\hat{\rho}_i$ becomes non-Hermitian. Clearly, in this case, in order to ensure Hermiticity of the total density matrix $\hat{\rho}(t)$ one has to consider the Hermitian symmetric $\hat{\rho}_i^{\mathrm{s}} = \hat{\rho}_i + \hat{\rho}_i^\dagger$ and antisymmetric $\hat{\rho}_i^{\mathrm{a}} = i\left(\hat{\rho}_i - \hat{\rho}_i^\dagger\right)$ combinations. Again, by performing the same decomposition procedure as above, one arrives at the density matrices

$$\hat{\rho}_i^{\mathrm{s}} = \hat{\rho}_i^{\mathrm{s}+} - \hat{\rho}_i^{\mathrm{s}-}, \quad \text{and} \quad \hat{\rho}_i^{\mathrm{a}} = \hat{\rho}_i^{\mathrm{a}+} - \hat{\rho}_i^{\mathrm{a}-}. \tag{14}$$

In this formalism, a Liouvillian exceptional point (LEP) is the point of the parameter space where two eigenmatrices of the Liouvillian coalesce. Since LEPs are associated with a non-diagonalizable Liouvillian, at the critical point one has a Jordan canonical form. With an LEP of order 2, one has an eigenvalue λ_{EP} and a generalized eigenmatrix $\hat{\rho}'_{\mathrm{EP}}$. Consequently, Eq. (10) becomes:

$$\hat{\rho}(t) = \sum_i c_i(t)\hat{\rho}_i + c_{\mathrm{EP}}(t)\hat{\rho}_{\mathrm{EP}} + c'_{\mathrm{EP}}(t)\hat{\rho}'_{\mathrm{EP}}, \tag{15}$$

where

$$c_{\mathrm{EP}}(t) = \exp(\lambda_{\mathrm{EP}}t)\,\mathrm{Tr}[\hat{\sigma}_{\mathrm{EP}}\hat{\rho}(0)],$$

while

$$c'_{\mathrm{EP}}(t) = t\exp(\lambda_{\mathrm{EP}}t)\,\mathrm{Tr}[\hat{\sigma}'_{\mathrm{EP}}\hat{\rho}(0)].$$

Moreover, LEPs should be understood as purely dynamical phenomena. In this Lindblad ME formalism, LEPs can emerge only for those eigenstates of the Liouvillian with a negative real part, i.e., those describing the evolution of an initial density matrix towards its steady state (for more detailed discussions, see Refs. [43, 45, 48]).

2. *Two-time correlation functions*

A direct diagonalization of the Liouvillian necessary to access its spectrum, however, is often extremely challenging; especially, considering the exponentially diverging size of the Hilbert space of the system. A two-time correlation function (TTCF) could capture the nature of EPs: a generic operator $\hat{O}$, which does not commute with the Hamiltonian, projects the system *out* of its steady state. This new density matrix is the superposition of several Liouvillian eigenmatrices, in principle including those associated with a LEP. For example, this idea was used in Ref. [57] to explicitly access the Liouvillian gap (i.e., the λ_i with smallest real part) of a Kerr resonator. This implies that the conditional dynamics, which follows the application of the operator $\hat{O}$, bears a signature of the EP presence. Indeed, any TTCF can be written as [58]:

$$\langle\hat{A}(t)\hat{B}(t+\tau)\rangle = \mathrm{Tr}\left\{\hat{A}(0)e^{\mathcal{L}\tau}\left[\hat{\rho}(t)\hat{B}(0)\right]\right\}, \tag{16}$$

where the square bracket indicates that the action of the exponential Liouvillian map must be taken on the matrix $\rho(t)\hat{B}(0)$. In this regard, for the steady state, we define

$$\langle \hat{A}(0)\hat{B}(\tau)\rangle_{\rm ss} = {\rm Tr}\left\{\hat{A}(0)e^{\mathcal{L}\tau}\left[\hat{\rho}_{\rm ss}\hat{B}(0)\right]\right\}. \tag{17}$$

The matrix $\hat{\rho}_{\rm ss}\hat{B}$ is, in general, different from $\hat{\rho}_{\rm ss}$. Therefore, we can express it in terms of the generalized eigenmatrices $\hat{\rho}_i$ of the Liouvillian (i.e., including $\hat{\rho}'_{\rm EP}$), that is

$$\hat{\rho}_{\rm ss}\hat{B} = \sum_i c_i\hat{\rho}_i. \tag{18}$$

Because we have used the spectral decomposition of the Liouvillian, and by recalling the linearity of the trace, we have

$$\langle \hat{A}(0)\hat{B}(\tau)\rangle_{\rm ss} = \sum_i c_i {\rm Tr}\left\{\hat{A}(0)e^{\mathcal{L}\tau}\left[\hat{\rho}_i\right]\right\}. \tag{19}$$

We have two possible cases: (i) For a system without EPs or away from them, the Eq. (19) reads

$$\langle \hat{A}(0)\hat{B}(\tau)\rangle_{\rm ss} = \sum_i c_i e^{\lambda_i\tau}{\rm Tr}\left\{\hat{A}(0)\hat{\rho}_i\right\}. \tag{20}$$

Indeed, for long times, only the slow-decaying fields are relevant, and

$$\langle \hat{A}(0)\hat{B}(\tau)\rangle_{\rm ss} \simeq c_0{\rm Tr}\left\{A\hat{\rho}_0\right\} + c_1 e^{\lambda_1\tau}{\rm Tr}\left\{A\hat{\rho}_1\right\} + \dots \tag{21}$$

In this regard, $\langle \hat{A}(0)\hat{B}(\tau)\rangle_{\rm ss}$ as a function of time τ describes an exponential decay towards the steady-state value $c_0{\rm Tr}\left\{\hat{A}(0)\hat{\rho}_0\right\}$.
(ii) In the presence of an LEP, one has

$$\langle \hat{A}(0)\hat{B}(\tau)\rangle_{\rm ss} = \sum_i c_i\tau^{n_i}e^{\lambda_i\tau}{\rm Tr}\left\{\hat{A}(0)\hat{\rho}_i\right\}, \tag{22}$$

where n_i is the degree of the degeneracy of the EP associated with the eigenmatrix $\hat{\rho}_i$. For example, for an EP of degree 3, we would have a contribution of

$$\begin{aligned} e^{\lambda_i\tau}\Big[&c_i{\rm Tr}\left\{\hat{A}(0)\hat{\rho}_i\right\} + c_{i+1}\tau{\rm Tr}\left\{\hat{A}(0)\hat{\rho}_{i+1}\right\} \\ &+c_{i+2}\tau^2{\rm Tr}\left\{\hat{A}(0)\hat{\rho}_{i+2}\right\}\Big], \end{aligned} \tag{23}$$

in the expansion of Eq. (19).

In this regard, a deviation from an exponential decay signals the presence of an EP. This implies that the conditional dynamics, which follows the application of the operator $\hat{O}$, bears a signature of the presence of an EP.

III. HAMILTONIAN AND LIOUVILLIAN EXCEPTIONAL POINTS IN THE SEMICLASSICAL REGIME

Here, we study the EPs of both non-Hermitian Hamiltonian and Liouvillian in the semiclassical limit. Hence, we consider the two-cavity system, shown in Fig. 1, populated by many photons $\langle\hat{n}\rangle \gg 1$, i.e., the system can be probed by intense coherent fields. Such an assumption does not allow us to represent the Liouvillians in their matrix form, due to the rapidly exponentially diverging size of the latter. The weak-gain case, where the Liouvillian can be exactly diagonalized, will be investigated in Sec. IV. Here, instead, we resort rather to the two-mode formalism to deduce the presence of an LEP.

♣ We note that the effective Hamiltonian, studied here, describes the gain and loss as the imaginary parts of the frequencies of quantum fields [see Eq. (8)]. Such a Hamiltonian arises from the mean-field approximation and, as a result, its use is justified in the semiclassical regime, when considering intense coherent fields. The NHH associated with this model explicitly exhibits a $U(1)$ Hamiltonian symmetry, implying that the subspaces corresponding to different numbers of excitations do not mix, even if the total number of excitations is not conserved. On the other hand, this symmetry is broken in the corresponding Liouvillian because of the presence of the quantum-jump terms. The Liouvillian approach describes a mixed-state dynamics obtained by averaging over many pure-state quantum trajectories, where quantum jumps induce transitions between manifolds corresponding to different numbers of excitations. Nonetheless, in the semiclassical limit with many excitations, the action of the creation and annihilation operators, associated with a quantum jump, scales as $\sqrt{n}$ in a cavity with n excitations, while the other energy terms scale as n. Therefore, adding or removing a single excitation does not drastically change typical properties of the system even at the level of its eigenvectors. As a result, in the frequency spectrum, one might expect some similarity between an NHH and the corresponding Liouvillian in the semiclassical limit.

A. Hamiltonian exceptional points

Let us first find an EP of the effective NHH $\hat{H}_{\rm eff}$, in Eq. (8).

By introducing the operator vector $\hat{a} = (\hat{a}_1, \hat{a}_2)^T$, one can recast the NHH $\hat{H}_{\rm eff}$, in Eq. (8), in the matrix form as follows

$$\hat{H}_{\rm eff} = \hat{a}^\dagger H\hat{a}, \quad \text{where} \quad H = \begin{pmatrix} \omega_c + i\frac{A-\Gamma_1}{2} & -i\kappa \\ i\kappa & \omega_c - i\frac{\Gamma_2}{2}\end{pmatrix}, \tag{24}$$

From Eq. (24), one then can immediately find the eigenvalues of the Hamiltonian $\hat{H}_{\rm eff}$

$$\nu_{1,2} = \omega_c + \frac{i}{4}(A-\Gamma_+) \pm \frac{i}{4}\beta, \tag{25}$$

where $\beta = \sqrt{(A-\Gamma_-)^2 - 16\kappa^2}$, and $\Gamma_\pm = \Gamma_1 \pm \Gamma_2$.

♣ The complex eigenvalues ν_i indicate the non-Hermitian character of the Hamiltonian $\hat{H}_{\rm eff}$. Moreover, because of this non-Hermiticity, the operator $\hat{H}_{\rm eff}$ can at-

tain both right $|\psi\rangle$ and left $\langle\tilde{\psi}|$ eigenvectors via relations

$$\hat{H}_{\rm eff}|\psi_i\rangle = \nu_i|\psi_i\rangle \quad \text{and} \quad \langle\tilde{\psi}_i|\hat{H}_{\rm eff} = \nu_i\langle\tilde{\psi}_i|, \tag{26}$$

respectively. Hereandafter, without loss of generality, we consider only right eigenvectors $|\psi_i\rangle$ of the NHH $\hat{H}_{\rm eff}$, since the HEPs are defined equivalently using either set of vectors.

The corresponding right eigenvectors become

$$|\psi_{1,2}\rangle = \frac{1}{N_{1,2}}\begin{pmatrix} A-\Gamma_- \pm \beta \\ 4\kappa \end{pmatrix}, \tag{27}$$

where $N_\pm$ is the corresponding normalization coefficient.

By analyzing Eqs. (25) and (27), one comes to the conclusion that, in the semiclassical regime, the NHH $\hat{H}_{\rm eff}$ has an HEP, where both eigenvalues and eigenvectors coalesce when

$$\kappa^{\rm s}_{\rm HEP} = \frac{1}{4}\left|A-\Gamma_-\right|. \tag{28}$$

♣ At the HEP, the two linearly independent eigenvectors $|\psi_{1,2}\rangle$ coalesce to a single eigenvector

$$|\psi_{\rm HEP}\rangle \equiv \begin{pmatrix} 1 \\ 1 \end{pmatrix}. \tag{29}$$

In this case, the 2×2 NHH $\hat{H}_{\rm eff}$ becomes non-diagonazible, thus, acquiring a Jordan form. This means that, at the HEP, the generalized eigenspace of the NHH $\hat{H}_{\rm eff}$ is spanned by the vector $|\psi_{\rm HEP}\rangle$ and a pseudo-eigenvector $|\psi'_{\rm HEP}\rangle$, obtained from $|\psi_{\rm HEP}\rangle$ via a Jordan chain relation, and which reads as:

$$|\psi'_{\rm HEP}\rangle \equiv \begin{pmatrix} -1 \\ 1 \end{pmatrix}. \tag{30}$$

For details regarding pseudo-eigenvectors see, e.g., Refs. [59, 60].

It is also worth noticing that the NHH $\hat{H}_{\rm eff}$ in Eq. (8) fails to incorporate spontaneous emission, since $\hat{H}_{\rm eff}|0\rangle = 0$. Obviously, because of the presence of the gain process in the active cavity, the probability of spontaneous emission is nonzero. To overcome this difficulty, one can apply the Heisenberg equations to the quantum field operators $\hat{a}_j$ $(j=1,2)$:

$$\frac{{\rm d}\hat{a}_j}{{\rm d}t} = \frac{1}{i\hbar}[\hat{a}_j, \hat{H}_{\rm eff}],$$

with the phenomenologically introduced quantum Langevin forces [61],

$$\begin{aligned}
\frac{\rm d}{{\rm d}t}\hat{a}_1 &= \frac{A-\Gamma_1}{2}\hat{a}_1 - \kappa\hat{a}_2 + \sqrt{A}\hat{g}_1^\dagger + \sqrt{\Gamma_1}\hat{l}_1, \\
\frac{\rm d}{{\rm d}t}\hat{a}_2 &= -\frac{\Gamma_2}{2}\hat{a}_2 + \kappa\hat{a}_1 + \sqrt{\Gamma_2}\hat{l}_2,
\end{aligned} \tag{31}$$

where $\hat{g}_j^\dagger$ $(\hat{l}_j)$ is the quantum noise amplification (dissipation) operator of the jth cavity, with the commutation relations $[\hat{O}_j(t), \hat{O}_k^\dagger(t')] = \delta_{jk}\delta(t-t')$, for $\hat{O} = \hat{g}, \hat{l}$, $j=1,2$.

Now, the equations of motion for the quantum fields given in Eq. (31) can provide the same fields dynamics as by the Liouvillian $\mathcal{L}$ [39], which we consider below.

Importantly, in order to properly describe the spectral properties of the fields, the rate equations in Eq. (31), for the active cavity field $\hat{a}_1$, should contain both amplification and dissipation noise operators. Otherwise, one can arrive at wrong conclusions (see Appendix A for details). We stress that the omission of the dissipation noise operator in the active cavity, in Eq. (31), has become widespread in the literature, especially in that devoted to $\mathcal{PT}$-symmetric systems.

B. Liouvillian exceptional points

As we discussed, it is, in general, challenging to find an LEP of the Liouvillian $\mathcal{L}$ in Eq. (7), especially in the semiclassical regime. However, one could infer the presence of LEPs using the TTCFs of the fields, as it was described in Sec. II B. Below, we compute $\langle\hat{a}_j^\dagger(0)\hat{a}_j(\tau)\rangle_{\rm ss}$ for the field in the jth cavity, $j=1,2$, in the steady state, to demonstrate its ability to capturing the EPs of the Liouvillian. We note that this method, which enables to reveal the dynamics of the Liouvillian, can be extended to high-order TTCFs [62], as it was experimentally done in, e.g., Ref. [57]. Moreover, our calculations are made simpler by the absence of a driving field in the Eq. (1), i.e., the TTCF does not involve a coherent part due to an external driving laser field, and will only capture the incoherent part of the TTCF induced by the gain in the active cavity. We note that, in the presence of a coherent field, the dynamical character of the incoherent part of the TTCF would not change qualitatively; thus, we could perform the same analysis for that model. Finally, we stress that this method indicates the presence of an LEP, but it does not provide neither the structure of the eigenmatrices of the Liouvillian nor their relation to the eigenvectors of the NHH. These two can differ substantially, as it will be shown in the next section.

1. *Computation of the two-time correlation function*

To obtain the TTCF one may invoke the quantum regression theorem, which states that the equations of motion for system operators are also the equations of motion for their correlation functions. To express this theorem mathematically, one can write the following equation [63]:

$$\frac{d}{d\tau}\langle\hat{O}(t)\hat{\boldsymbol{A}}(t+\tau)\rangle = \boldsymbol{M}\langle\hat{O}(t)\hat{\boldsymbol{A}}(t+\tau)\rangle, \tag{32}$$

where $\hat{\boldsymbol{A}} = [\hat{A}_1, \hat{A}_2, \ldots, \hat{A}_\nu]$ is the vector of a complete set of the system operators $\hat{A}_\mu$, in the sense that the averages $\langle\hat{A}_\mu\rangle$, $\mu = 1,2,\ldots,\nu$, form the set of coupled linear

equations with the evolution matrix $\boldsymbol{M}$. The operator $\hat{O}$ can be arbitrary, not necessarily belonging to $\hat{A}_\mu$.

For the studied system of coupled active and passive cavities, governed by a ME with the Liouvillian $\mathcal{L}$ in Eq. (7), and with the Hamiltonian in Eq. (1), the complete set is formed by the following vector $\hat{\boldsymbol{A}} = [\hat{a}_1, \hat{a}_2]$ of the field operators $\hat{a}_1, \hat{a}_2$. The evolution matrix $\boldsymbol{M}$ is found to be

$$\boldsymbol{M} = -iH, \tag{33}$$

where H is given in Eq. (24).

Now, by combining Eqs. (32) and (33), and using the operators $\hat{a}_j^\dagger$, $j = 1, 2$ instead of the operator $\hat{O}$, one obtains the following solution for the TTCF,

$$\begin{pmatrix} \langle \hat{a}_j^\dagger(t)\hat{a}_j(t+\tau)\rangle \\ \langle \hat{a}_j^\dagger(t)\hat{a}_k(t+\tau)\rangle \end{pmatrix} = \exp(\boldsymbol{M}\tau) \begin{pmatrix} \langle \hat{a}_j^\dagger(t)\hat{a}_j(t)\rangle \\ \langle \hat{a}_j^\dagger(t)\hat{a}_k(t)\rangle \end{pmatrix}, \tag{34}$$

for $j, k = 1, 2$, $j \neq k$.

The TTCF in the steady state can be obtained by sending $t \to \infty$ in Eq. (34). As Eq. (34) indicates, in order to find correlation functions, one needs first to know the averages of the photon numbers in each cavity as well as the averages $\langle \hat{a}_j^\dagger(t)\hat{a}_k(t)\rangle$.

Again, by applying the master equation in Eq. (7) to the operators $\hat{a}_j^\dagger\hat{a}_k$ and $\hat{a}_j^\dagger\hat{a}_k$, one obtains their averages in the steady state as follows:

$$\begin{aligned} \langle \hat{a}_1^\dagger\hat{a}_1\rangle_{\rm ss} &= A\left(4\kappa^2 - G_1\Gamma_2 + \Gamma_2^2\right)f, \\ \langle \hat{a}_2^\dagger\hat{a}_2\rangle_{\rm ss} &= 4\kappa^2 A f, \\ \langle \hat{a}_1^\dagger\hat{a}_2\rangle_{\rm ss} &= \langle \hat{a}_2^\dagger\hat{a}_1\rangle_{\rm ss} = 2\kappa\Gamma_2 A f, \end{aligned} \tag{35}$$

where $G_1 = A - \Gamma_1$ represents the total net gain in the active cavity, and $f^{-1} = \left(4\kappa^2 - G_1\Gamma_2\right)\left(\Gamma_2 - G_1\right)$ is a normalization factor.

As an example, in Fig. 2 we plot the averages of the photon numbers in the steady state in both cavities given in Eq. (35), as a function of the intercavity coupling strength κ. The system is chosen to balance *intrinsic* gain and losses , i.e., one imposes the condition $A - C_1 - C_2 = 0$ simulating the *effective* $\mathcal{PT}$-symmetric regime [4]. Such a symmetry is called *effective* since the *total* gain and losses are not balanced due to nonzero waveguide coupling $\gamma \neq 0$; thus, breaking the genuine $\mathcal{PT}$-symmetry (for details see also Ref. [64]). As Fig. 2 indicates, the average steady-state number of photons in both cavities can be large, due to the interplay between spontaneous emission and the gain in the active cavity [c.f. Eq. (35)]. By varying the coupling strength κ between the cavities, one obtains different values of the photon numbers in the resonators, which become identical in the limit $\kappa \to \infty$ (see Fig. 2):

$$\langle \hat{n}_1\rangle = \langle \hat{n}_2\rangle = \frac{A}{\Gamma_+ - A}.$$

Photon number fluctuations are large too. For instance, for $\kappa = 0$, the dispersion of the number of photons in the active cavity becomes $\sigma(\langle \hat{n}\rangle) = \sqrt{\Gamma_1/A}\langle \hat{n}\rangle$, which indicates the thermal character of the gain.

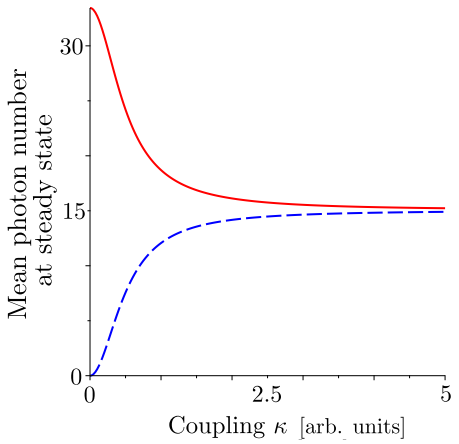

FIG. 2. Mean photon-numbers $\langle \hat{n}_1\rangle$ in the active cavity (red solid curve) and $\langle \hat{n}_2\rangle$ in the passive cavity (blue dashed curve) in the steady state as a function of the intercavity coupling κ. The intrinsic gain and loss are balanced in the system, i.e., to satisfy the condition $A - C_1 - C_2 = 0$, where the gain $A = 30.1$ [arb. units], the intrinsic loss in the passive cavity $C_2 = 0.1$ [arb. units], and the coupling of both cavities to the waveguides as $\gamma = 1$ [arb. units] (see Fig. 1).

Now, combining together Eqs. (34) and (35), one arrives at the formula for the TTCF in both cavities in the steady state, *and away from the LEP*, which writes:

$$\begin{aligned} \langle \hat{a}_1^\dagger(0)\hat{a}_1(\tau)\rangle_{\rm ss} &= u_2\exp(-i\nu_1\tau) + u_1\exp(-i\nu_2\tau), \\ \langle \hat{a}_2^\dagger(0)\hat{a}_2(\tau)\rangle_{\rm ss} &= v_2\exp(-i\nu_1\tau) + v_1\exp(-i\nu_2\tau), \end{aligned} \tag{36}$$

where $\nu_{1,2}$ are the eigenfrequencies of the NHH in Eq. (25), and $u_{1,2}$, $v_{1,2}$ are functions of the system parameters given in Appendix B.

Equation (36) implies that the dynamics of the TTCF, away from the LEP, imposed by the Liouvillian is similar to that of the NHH $\hat{H}_{\rm eff}$ imposed on the fields. By comparing Eq. (36) and Eq. (21), one can see that the rate of decay of these TTCF is exactly captured by the NHH. Most importantly, as it follows from Eq. (36), the position of at least one of the LEPs coincides with that of the HEP:

$$\kappa^{\rm s}_{\rm LEP} = \kappa^{\rm s}_{\rm HEP} = \frac{1}{4}\left|A - \Gamma_-\right|. \tag{37}$$

♣ When $\kappa < \kappa^{\rm s}_{\rm LEP}$, the TTCFs in Eq. (36) exhibit a simple exponential decay, as described by a superposition of two exponents of the Liouvillian eigenvalues ν_1 and ν_2.

When the intercavity coupling κ equals $\kappa^{\rm s}_{\rm LEP}$, by considering a rotating reference frame at the cavity frequency ω_c, the TTCFs in Eq. (36) reduce to:

$$\langle \hat{a}_i^\dagger(0)\hat{a}_i(\tau)\rangle_{\rm ss} = \exp\left(\frac{1}{4}\lambda\tau\right)(P_i + Q_i\tau), \quad i = 1, 2, \tag{38}$$

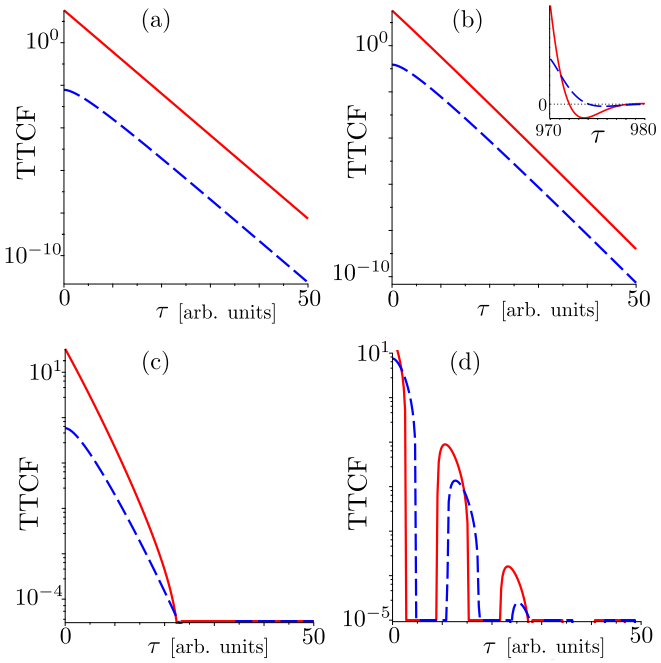

FIG. 3. Two-time correlation function $\langle \hat{a}_j^\dagger(0)\hat{a}_j(\tau)\rangle_{\rm ss}$ in the steady state, according to Eq. (36), in the rotating reference frame ω_c, for the active (red solid curve) and passive (blue dashed curve) cavities, for different values of the intercavity coupling κ: (a) $\kappa = 0.01$ [arb. units], (b) $\kappa = 0.0501$ [arb. units], (c) $\kappa = 0.1$ [arb. units], and (d) $\kappa = 0.5$ [arb. units]. The other system parameters are the same as in Fig. 2. For this system, the Liouvillian EP is found at $\kappa = 0.05$ [arb. units], according to Eq. (36), i.e., the point at and above which the TTCF fails to demonstrate solely an exponential decay [see the inset in panel (b)]. In order to capture the deviation of the TTCF from the explicit exponential behaviour right above the EP, one might need longer correlation times τ [see the inset in panel (b)]. All panels are shown in a logarithmic scale, except the inset in panel (b).

where $\lambda = A - \Gamma_+ < 0$, and the values of the constants P_i and Q_i are given in Appendix B. We just note here that the expressions for $P_{1,2}$ and Q_2 are always positive-valued, whereas the values of Q_1 can be either positive or negative, ♣ depending on whether the expression $A - \Gamma_-$ is positive or negative, respectively (see Appendix B, for details). Thus, for linear systems with the $\mathcal{PT}$-symmetry, including the *effective* $\mathcal{PT}$-symmetry, the coefficient Q_1 is always positive and becomes proportional to the intercavity-coupling strength κ. To experimentally determine a LEP from the TTCFs in Eq. (38), one might need to implement curve fitting techniques to capture the deviation of the TTCF from a simple exponential decay, when increasing the intercavity coupling κ. In particular, if $A - \Gamma_- < 0$, i.e., $Q_1 < 0$, then a LEP can be directly defined from the arising negative values of the TTCF in the active cavity, according to Eq. (38).

On the other hand, in general, right above the EP, i.e., when $\kappa > \kappa_{\rm LEP}^{\rm s}$, both TTCFs in Eq. (36) can acquire negative values due to the arising oscillatory term β in the rotating frame ω_c. In order to catch these arising negative values in the TTCFs, the observation of longer coherence times might be needed [see the inset in Fig. 3(b)]. Additionally, these oscillations make the TTCFs substantially deviate from the simple exponential decay when increasing κ [see Figs. 3(c)–3(d)].

2. *Power spectrum*

We note that in real experimental situations, it might be very challenging to measure a TTCF, necessary to determine the exact position of the LEP. In this case, one can use complementary frequency space analysis, where instead of the TTCF, one just measures the power spectra of the detected fields. Those power spectra can provide an intuitive and comprehensive interpretation of the EP. Namely, the presence of the EP, e.g., of the second order, can be revealed by a squared Lorentzian lineshape in the power spectrum, corresponding to a coalescence of two resonance peaks. The latter technique has been already successfully used in, e.g., Ref. [11].

The formula for the power emission spectra in the jth cavity expressed via the TTCF reads

$$S_j(\omega) = \frac{1}{2\pi}\int_{-\infty}^{\infty} \langle \hat{a}_j^\dagger(0)\hat{a}_j(\tau)\rangle_{\rm ss} e^{i\omega\tau} {\rm d}\tau. \tag{39}$$

By combining Eqs. (33)–(35) and (39), one obtains the emission spectra in the active and passive cavities:

$$S_1(\omega) = \frac{AF}{2\pi}\left[\Delta^2 + \frac{\Gamma_2^2}{4}\right], \quad S_2(\omega) = \frac{\kappa^2 AF}{2\pi}, \tag{40}$$

where

$$F = \left[\omega_+^2\omega_-^2 + \tfrac{1}{4}(G_1^2+\Gamma_2^2)\Delta^2 + \tfrac{1}{16}G_1\Gamma_2(G_1\Gamma_2 - 8\kappa^2)\right]^{-1},$$

with $\Delta = \omega - \omega_c$ being the frequency detuning, $\omega_\pm = \Delta \pm \kappa$, and the net gain in the active cavity is $G_1 = A - \Gamma_1 < 0$.

♣ Before we start the spectral-power analysis based on Eq. (40), first we would like to draw a small remark. Note that because of our definition of the power spectra given in terms of the non-Hermitian annihilation operators $\hat{a}$ in Eq. (39), the spectrum of the vacuum is set to zero [39, 65]. The quantum-field spectral power $S(\omega)$ vanishes for the vacuum, as implied by Eq. (37). Indeed, the spectral power is defined as the Fourier transform of a two-time average of the non-Hermitian boson operators $\hat{a}$ and $\hat{a}^\dagger$. In this case, the spectral power becomes proportional to the mean photon number in the steady state, which for the vacuum is zero, regardless of the presence of the dissipation noise operators. On the other hand, when performing a real experiment, one measures the spectrum of the Hermitian electric field $\hat{\mathcal{E}} \equiv \hat{a} + \hat{a}^\dagger$, which for the vacuum in the cavity with frequency ω_0 and loss rate Γ gives the following nonvanishing spectral power:

$$S_{\hat{\mathcal{E}}}(\omega) \equiv \int \langle \hat{\mathcal{E}}(0)\hat{\mathcal{E}}(\tau)\rangle \exp(i\omega\tau){\rm d}\tau = \frac{\Gamma}{(\omega-\omega_c)^2 + \frac{\Gamma^2}{4}},$$

where the amplitude of the vacuum fluctuations is set to 1.

Now, by inspecting Eq. (40), one can see that the emission spectra in both cavities are provided mainly by the gain A. In particular, for a fixed intercavity coupling κ, both power spectra $S_1(\omega) \to 0$ and $S_2(\omega) \to 0$, if $A \to 0$. On the other hand, the power spectrum S_2 in the passive cavity is always zero, whenever $\kappa = 0$, regardless of the values of the gain A in the active cavity, as expected. Moreover, the derived formulas in Eq. (40) show that the emission spectra in both cavities are, in general, squared Lorentzians [66]. The latter confirms that the system can experience a mode-splitting phenomenon, i.e., there is a point in parameter space where two resonances coalesce.

The mode splitting, i.e., the appearance of the squared Lorentzians, occurs at different κ for the two cavities, and it is defined via (see Appendix B for details):

$$\kappa_1 = \frac{\sqrt{\Gamma_2}}{2}\left[\sqrt{(G_1-\Gamma_2)^2+\Gamma_2^2}+(G_1-\Gamma_2)\right]^{\frac{1}{2}},$$
$$\kappa_2 = \frac{\sqrt{2}}{4}\sqrt{G_1^2+\Gamma_2^2}. \tag{41}$$

♣ This mode-splitting difference is due to the fact that the system has an *effective* $\mathcal{PT}$-symmetry. This means that the uncompensated losses, due to the coupling of the cavities to the waveguides, affect the two mode resolution in both cavities at the same value of κ. Moreover, the larger is the uncompensated loss, the larger is the mode-splitting difference.

A comparison of Eqs. (37) and (41) leads us to the conclusion that the LEPs, which are exactly determined from the TTCF, and those obtained via power-spectra analysis are, in general, are different.

These spectral bifurcation points (SBPs) of power spectra, given in Eq. (41), converge to the LEP defined from the TTCF in Eq. (37) only in the limit when the total loss and gain in the system become balanced, i.e, when $(A-\Gamma_1-\Gamma_2) \to 0$. This means that the extra losses induced by the imbalance of the net gain and damping in the active and passive cavities strongly affects the resolution of the genuine LEP exploiting the power spectrum. We also remark that, in the limit when $(A-\Gamma_1-\Gamma_2) \to 0$, the active cavity approaches the lasing threshold, where the system linearity assumption can, in general, fail, and possibly lead to nonphysical results. Hence, since the "true" LEP is captured by the TTCF, the SBPs can be seen as an approximation of the LEP.

Nevertheless, the analysis of the power spectra can give us some additional and valuable hints to understand the physics of the system. In Fig. 4 we plot the power spectra of both cavities for different values of the intercavity coupling κ. In Fig. 5, instead, we plot the peaks of the power spectra resonances (whose splitting signaling the SBPs) and the imaginary part of $\nu_{1\,2}$ associated to the decay of the TTCF (whose bifurcation indicates the LEP). We chose balanced intrinsic gain and losses $A - C_1 - C_2 = 0$ (which is the effective $\mathcal{PT}$-symmetric regime). Thanks

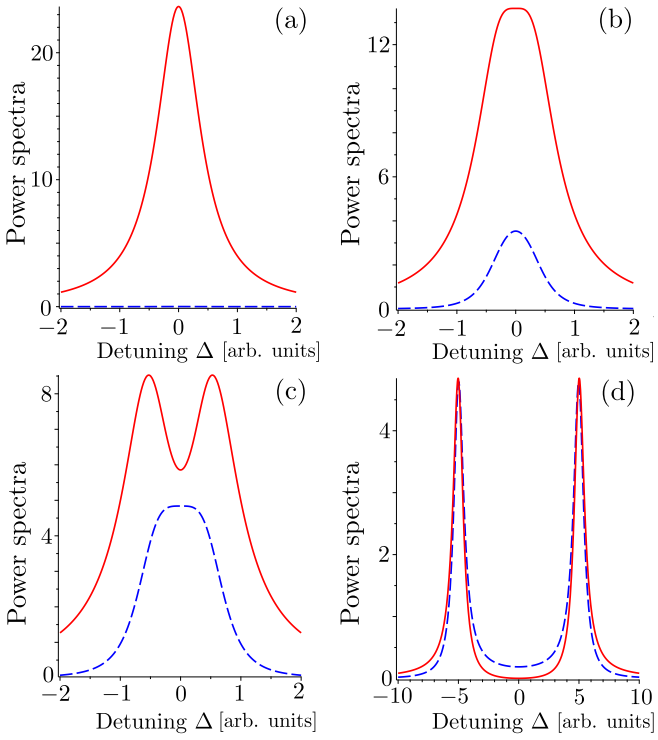

FIG. 4. Power spectra $S_j(\omega)$, according to Eq. (40), in the active (red solid curve) and passive (blue dashed curve) cavities versus the frequency detuning $\Delta = \omega - \omega_c$ for different values of the intercavity coupling κ: (a) $\kappa = 0.1$ [arb. units], (b) $\kappa = 0.278$ [arb. units], (c) $\kappa = 0.5$ [arb. units], and (d) $\kappa = 5$ [arb. units]. We assumed that the system has an intrinsic balanced gain and losses satisfying the relation $A - C_1 - C_2 = 0$. The system parameters are the same as in Fig. 2. Near SBPs, given in Eq. (41), the spectra exhibit squared Lorentzian lineshapes [see panels (b)-(c)]. While far away from the SBPs, the spectra are Lorentzian with one peak below the SBPs, and two peaks above the SBPs [see panels (a) and (d)]. This figure demonstrates that, in general, the Liouvillian EP can not be faithfully determined from the power-spectra analysis, in contrast to the TTCF, shown in Fig. 3.

to the additional coupling of the cavities to the waveguides, the total gain in the system becomes smaller than the total loss i.e., $A - \Gamma_1 - \Gamma_2 = A - C_1 - C_2 - 2\gamma < 0$. Our formalism remains valid for γ large enough to ensure that the active cavity is far below the lasing threshold. As one can see, for very small values of κ, the power spectrum in both cavities is asymmetric, i.e., the emission is mainly observed in the active cavity, which has a Lorentzian shape [see Fig. 4(a)]. This is because the coupling is too small for the generated photons in the active resonator to pass into the passive cavity and be emitted. Again, this is a demonstration of the impossibility to realize $\mathcal{PT}$-symmetry in photonic systems due to a spontaneous emission enhanced by the gain A. If one were to drive the system by intense classical fields, this would eventually restore the symmetry, but completely conceal the presence of the spontaneous-emission

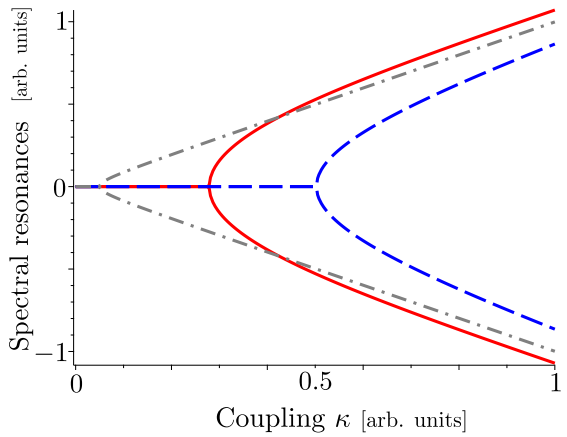

FIG. 5. The resonances of the power spectra in the active (red solid curve) and passive (blue dashed curve) cavities from Fig. 4 (see also Appendix B, for details). The system parameters are the same as in Fig. 2. There is a shift between mode splittings in the two cavities, which is increasing with increasing value of waveguide couplings $\gamma_1 = \gamma_2 = \gamma$. For comparison, the imaginary frequencies $\nu_{1,2}$ of the Liouvillian (grey dash-dotted curves), which are the same as the real frequencies of the NHH given in Eq. (25), are also displayed on the graph. The imaginary frequencies of the Liouvillian and resonances of the emission spectra coincide in the limit $\kappa \to \infty$. On the other hand, the LEP of $\mathcal{L}$ in Eq. (37) and SBPs of $S_{1,2}$ in Eq. (41) tend to coincide in the limit $A - \Gamma_1 - \Gamma_2 \to 0$, i.e., in the limit where the assumption of the linearity of the system can fail.

fields. Note that similar conclusions, regarding the self-sustained radiation in the system and observed asymmetry in the emission spectra, have been previously obtained in Ref. [66, 67] by applying scattering theory.

By increasing the coupling strength κ, the emission spectrum in the active cavity start exhibiting a squared-Lorentzian lineshape [see Fig. 4(b)], which signals the arising mode splitting in the active resonator, i.e., the appearance of an SBP in the system (see Fig. 5). At the same time, the emission spectrum in the passive cavity becomes comparable in power to the power spectrum in the active resonator but with a Lorentzian lineshape [see Figs. 4(b) and 5]. Further increasing κ leads to a clear mode splitting in the active resonator and the emergence of a squared-Lorentzian line in the passive resonator [see Fig. 4(c) and 5]. For even larger values of κ, S_1 and S_2 are Lorentzian and coincide with each other, showing two well-separated lines, which, in the limit $\kappa \to \infty$, become proportional to the intercavity splitting κ [see Fig. 4(d) and 5].

3. *Discussion about the semiclassical limit*

In summary of this section, we have defined and compared the HEP and one of the LEPs in the semiclassical regime. Whereas the HEP has been directly obtained from the spectra of the NHH, the LEP has been determined from the TTCF, which enables to detect well the LEPs in the system. The analysis provided implies that, in this regime, both HEP and, at least, one of the LEPs appears for the same combination of system parameters and has the same decay rate. We note that although, in general, one fails to identify the exact value of an LEP from the power spectra based on the resonant peaks splitting, it might be possible to detect it by utilizing other statistical measures applied to the spectra curves, e.g., such as bimodal coefficients or Binder cumulants. This study, however, is beyond the scope of this work. Finally, in the special cases when the system approaches the genuine $\mathcal{PT}$-symmetry with balanced total gain and losses in both cavities, the mode splitting phenomenon in the power spectra tend to occur at the exact value of the LEP.

IV. HAMILTONIAN AND LIOUVILLIAN EXCEPTIONAL POINTS IN THE QUANTUM SINGLE-PHOTON LIMIT

Let us consider a situation when there is no more than one photon in each cavity, i.e., $\langle \hat{n}_i \rangle \ll 1$, $i = 1, 2$. This can be easily achieved when the ratio between the gain and the losses in the active cavity is very low, i.e., $A/\Gamma_1 \ll 1$, according to Eq. (35). In this case, the Hilbert space of the system can be reduced to a four dimensional space, spanned by the vectors $|j\rangle|k\rangle$ with $j, k = 0, 1$. As a result, we can easily represent both NHH and Liouvillian as small matrices, allowing their diagonalization and the study their EPs in the quantum single-photon limit.

A. Non-Hermitian Hamiltonian exceptional points

In the two-photon cutoff Hilbert space, the effective NHH in Eq. (8) attains the following matrix form (see Appendix C for details)

$$\hat{H}_{\text{eff}} \equiv \begin{pmatrix} 0 & & & \\ & \omega_c - i\frac{\Gamma_2}{2} & i\kappa & \\ & -i\kappa & \omega_c + \frac{i}{2}(A - \Gamma_1) & \\ & & & 2\omega_c + \frac{i}{2}(A - \Gamma_+) \end{pmatrix}, \tag{42}$$

with eigenvalues:

$$\eta_0 = 0, \quad \eta_1 = 2\omega_c + \tfrac{i}{2}(A - \Gamma_+), \quad \eta_{2,3} = \nu_{1,2}, \tag{43}$$

where $\nu_{1,2}$ are given in Eq. (25).

Note, that because of the resized NHH $\hat{H}_{\text{eff}}$, compared to that in Eq. (24), apart from the same eigenvalues $\eta_{2,3}$, this NHH has also two additional eigenvalues η_0 and η_1.

♣ Again, because the eigenvalues η_i, in Eq. (43), are complex, the NHH $\hat{H}_{\text{eff}}$ can attain both right and left eigenvectors.

♣ The right eigenvectors of the NHH $\hat{H}_{\rm eff}$, in Eq. (42), away from HEP, are

$$|\psi_0\rangle = |00\rangle, \quad |\psi_1\rangle = |11\rangle,$$
$$|\psi_{2,3}\rangle \equiv (A - \Gamma_- \pm \beta)|10\rangle + 4\kappa|01\rangle, \tag{44}$$

where β is given below Eq. (25). ♣ The normalization coefficients for the eigenstates $|\psi_{2,3}\rangle$, in Eq. (44), can be safely dropped, since the considered system in this quantum regime does not exhibit the $\mathcal{PT}$-symmetry, where the eigenstates might not be normalized [59].

♣ By inspecting Eq. (44), one can clearly see the coalescence of the eigenvalues $\eta_2 = \eta_3 = i(A - \Gamma_-)/4$, and that the eigenvectors $|\psi_2\rangle$ and $|\psi_3\rangle$ coalesce to the maximally entangled state $|\psi_{\rm HEP}\rangle \equiv |10\rangle + |01\rangle$, which occurs at the following HEP:

$$\kappa^{\rm q}_{\rm HEP} = \frac{1}{4}\left|A - \Gamma_-\right|. \tag{45}$$

As expected, for this NHH $\hat{H}_{\rm eff}$, the HEPs coincide in the semiclassical and single-photon limits.

♣ At the HEP, the NHH $\hat{H}_{\rm eff}$ becomes non-diagonazible, i.e., it attains a Jordan form. Hence, the generalized eigenspace of the NHH $\hat{H}_{\rm eff}$ consists of the the eigenvectors

$$|\psi_0\rangle = |00\rangle, \quad |\psi_1\rangle = |11\rangle, \quad |\psi_{\rm HEP}\rangle \equiv |10\rangle + |01\rangle, \tag{46}$$

and the singlet-type pseudo-eigenvector [59]:

$$|\psi'_{\rm HEP}\rangle \equiv |10\rangle - |01\rangle. \tag{47}$$

B. Liouvillian exceptional points

1. Eigenvalues

Within the two-photon approximation, the Liouvillian $\mathcal{L}$ in Eq. (7) is a 4×4 matrix. By combining together Eqs. (7) and (9), one obtains the following eigenvalues of $\mathcal{L}$ (see Appendix C for details):

$$\lambda_0 = 0, \quad \lambda_{1,2} = i\omega_c - \tfrac{1}{2}A_+ + \tfrac{1}{4}E_\pm,$$
$$\lambda_{3,4} = -\tfrac{1}{2}(A_+ \pm D), \quad \lambda_{5,6} = -\tfrac{1}{2}A_+,$$
$$\lambda_7 = 2i\omega_c - \tfrac{1}{2}A_+, \quad \lambda_{8,9} = i\omega_c - \tfrac{1}{2}A_+ - \tfrac{1}{4}E_\pm,$$
$$\lambda_{10} = -A_+, \quad \lambda_{11,12,13,14,15} = \lambda^*_{1,2,7,8,9}, \tag{48}$$

where $D = \sqrt{A_-^2 - 16\kappa^2}$, $A_\pm = A + \Gamma_\pm$,

$$E_\pm = \sqrt{2}\sqrt{(A+\Gamma_1)^2 + \Gamma_2^2 - 16\kappa^2 \pm F},$$

and

$$F = \left(A_+^2 A_-^2 + 16\kappa^2\left(8A\Gamma_2 - A_+^2\right)\right)^{\frac{1}{2}}.$$

♣ As an example, we plot the frequency spectrum λ_i of the Liouvillian in Fig. 6.

♣ Note that the Liouvillian frequency spectrum, in general, strongly depends on the interaction κ between the fields in the two cavities, particularly, when $\Gamma_i \gg \Gamma_j$, $i,j = 1,2$, $i \neq j$. It means that compared to the case when both cavities are isolated from each other, the decay rates λ_i of the Liouvillian states can either be substantially facilitated or impeded by this interaction [68–70].

2. Eigenmatrices

The eigenmatrices $\hat{\rho}_i$, corresponding to the real-valued eigenvalues λ_i, can be written as follows:

$$\hat{\rho}_j = \frac{1}{N_j}\begin{pmatrix} \rho_{00}^{(j)} & & & \\ & \rho_{01}^{(j)} & & \\ & & \rho_{10}^{(j)} & \\ & & & \rho_{11}^{(j)} \end{pmatrix}, \quad j = 0, 10, \tag{49}$$

$$\hat{\rho}_{3,4} = \begin{pmatrix} \rho'_{00} \pm f_1 D & & & \\ & \rho'_{01} \pm f_2 D & \rho'_{0110} \pm f_3 D & \\ & \rho'_{0110} \pm f_3 D & \rho'_{10} \pm f_4 D & \\ & & & \rho_{11} \end{pmatrix}, \tag{50}$$

$$\hat{\rho}_5 = \begin{pmatrix} \rho_{00} & & & \\ & \rho_{01} & \rho_{0110} & \\ & \rho_{0110} & \rho_{10} & \\ & & & \rho_{11} \end{pmatrix}, \quad \hat{\rho}_6 = \begin{pmatrix} 0 & & & \\ & \hat{\sigma}_y & & \\ & & & 0 \end{pmatrix}, \tag{51}$$

where D is given in Eq. (48), $\hat{\sigma}_y$ is 2×2 Pauli matrix, and the rest parameters are given in Appendix C.

The remaining non-Hermitian eigenmatrices with complex eigenvalues are the following:

$$\hat{\rho}_k = \begin{pmatrix} 0 & \rho_{0001}(\lambda_k) & \rho_{0010}(\lambda_k) & \\ & 0 & 0 & \rho_{0111} \\ & & 0 & \rho_{1011}(\lambda_k) \\ & & & 0 \end{pmatrix},$$
$$k = 1,2,8,9, \quad \text{and} \quad \hat{\rho}_7 = \begin{pmatrix} & & & 1 \\ & & & \\ & & & \\ & & & \end{pmatrix}, \tag{52}$$

and for the eigenvalues λ_l with $l = 11,12,13,14,15$, the eigenmatrices are found as a Hermitian conjugate of the eigenmatrices $\hat{\rho}_k$, with $k = 1,2,7,8,9$, respectively, where $\hat{\rho}_k$ are given in Eq. (52). The exact values of all the eigenmatrices in Eqs. (49)–(52) are given in Appendix C. Obviously, the spectrum of the Liouvillian $\mathcal{L}$ is much richer than that of the NHH $\hat{H}_{\rm eff}$.

3. Spectral decomposition and LEPs

♣ *(1) Study of* $\hat{\rho}_{0,10}$.— The Hermitian diagonal eigenmatrix $\hat{\rho}_0$, in Eq. (49), is the steady-state density matrix. As expected, the steady state is nothing else but a classical mixture of the states $|jk\rangle\langle jk|$, where $j,k=0,1$. The Hermitian eigenmatrix $\hat{\rho}_{10}$, instead, is responsible for the dynamical evolution of the diagonal elements $|jk\rangle\langle jk|$ towards the steady state with the decaying rate λ_{10}.

(2) Study of $\hat{\rho}_{3,4}$.— Let us now study the eigenmatrices $\hat{\rho}_{3,4}$, since, as it will be shown below, their eigenstates are the closest to those defined in Eq. (44).

♣ As it was stressed earlier, the EP of the Liouvillian is defined as a point in the parameter space where the eigenvalues and eigenmatrices of $\mathcal{L}$ coincide. By inspection of Eqs. (48) and (50), one can see that both eigenvalues $\lambda_{3,4}$ and corresponding eigenmatrices $\hat{\rho}_{3,4}$ coincide whenever $D=0$. Moreover, the eigenvalues $\lambda_{3,4}$ and eigenmatrices $\hat{\rho}_{3,4}$ coalesce with the eigenvalue λ_5, in Eq. (48), and the eigenmatrix $\hat{\rho}_5$, in Eq. (51), respectively. Therefore, the Liouvillian $\mathcal{L}$ acquires a third-order EP given by

$$\kappa^{\rm q}_{\rm LEP,1}=\frac{1}{4}|A_-|=\frac{1}{4}\left|A+\Gamma_1-\Gamma_2\right|. \tag{53}$$

The subscript 1 at $\kappa^{\rm q}_{\rm LEP,1}$ stands for the first LEP, since as it will be shown below, there are at least two LEPs in the system, and which in the limit $A\to 0$ coincide.

♣ Remarkably, despite the fact that the HEP $\kappa^{\rm q}_{\rm HEP}$ and LEP $\kappa^{\rm q}_{\rm LEP,1}$ are of different order and have a slightly different form (opposite signs at Γ_1 and Γ_2), they occur for the same combination of parameters in the weak-gain regime, where the two-photon cutoff can be safely applied. Namely, when considering a two-photon cutoff, one must bear in mind that the gain A in the active cavity should be very small compared to the total losses in the active cavity, i.e., $A/\Gamma_1\ll 1$, in order to justify the two-photon approximation. Therefore, in the case, when A becomes negligible compared to both Γ_1 and Γ_2, the LEP and HEP tend to coincide, i.e., $\kappa^{\rm q}_{\rm HEP}\cong\kappa^{\rm q}_{\rm LEP,1}$ (see also Fig. 6). Most importantly, our numerical results also indicate that even by increasing the gain A, and enlarging the subspace of the Hilbert space to higher-photon excitations, the LEP and HEP demonstrate the same tendency to overlap, i.e., $\kappa^{\rm q}_{\rm LEP,1}\to\kappa^{\rm q}_{\rm HEP}$ with increasing $\langle\hat{n}_1\rangle$ (see also Fig. 7). Therefore, the same EP can have *different* order for the NHH $\hat{H}_{\rm eff}$ and the Liouvillian $\mathcal{L}$.

♣ Note that the previous discussion can also be generalized if we consider a *truly* two coupled two-level system. Namely, if instead of considering the small-gain regime of a bosonic system we take under consideration a system where the photon-photon interaction determines a photon-blockade regime, the NHH not only fails to capture the nature of the LEP, but also the parameters for which it occurs.

When $\kappa<\kappa^{\rm q}_{\rm LEP,1}$, both eigenmatrices $\hat{\rho}_{3,4}$ are Hermitian, and one can immediately find their eigenstates as follows

$$\begin{aligned}
&|\psi_0^{(3,4)}\rangle=|00\rangle,\quad |\psi_1^{(3,4)}\rangle=|11\rangle,\\
&|\psi_{2,3}^{(3)}\rangle\equiv 4\kappa|01\rangle+\Big(D\pm|A_-|\Big)|10\rangle,\\
&|\psi_{2,3}^{(4)}\rangle\equiv 4\kappa|01\rangle+\Big(-D\pm|A_-|\Big)|10\rangle.
\end{aligned}\tag{54}$$

Direct inspection of Eq. (54) reveals that the subspace of the eigenstates of the density matrices $\hat{\rho}^{(2,3)}$ resembles the space of the eigenstates of the NHH $\hat{H}_{\rm eff}$ in Eq. (44). Moreover, in the limit $A\to 0$, this resemblence turns into equivalence.

♣ When $\kappa=\kappa^{\rm q}_{\rm LEP,1}$, then $\lambda_3=\lambda_4=\lambda_5=\lambda_{\rm EP}=-A_+/2$, and $\hat{\rho}_3=\hat{\rho}_4=\hat{\rho}_5$ (see also Fig. 6). The latter implies that the eigenstates of the Liouvillian at this LEP, which belong to the eigenmatrix $\hat{\rho}_5$ and describe the intercavity fields interaction, are the maximally entangled states, according to Eq. (59). Additionally, at the LEP $\kappa^{\rm q}_{\rm LEP,1}$, the algebraic multiplicity of the eigenvalue $\lambda_{\rm LEP}$ exceeds its geometric multiplicity, according to Eqs. (48), (50) and (51). Namely, the algebraic multiplicity of $\lambda_{\rm LEP}$ becomes four, but geometric multiplicity equals two, because there are only two linearly independent eigenmatrices $\hat{\rho}_{5,6}$ for this eigenvalue. The rank of the eigenmatrices $\hat{\rho}_{3,4,5}$ is the same and equals four, whereas the rank of the eigenmatrix $\hat{\rho}_6$ equals two. Therefore, one has to find two additional generilized pseudo-eigenmatrices of the rank four for the Liouvillian $\mathcal{L}$, which takes on a Jordan form in this case. These pseudo-eigenmatrices, denoted as $\hat{\rho}_5'$ and $\hat{\rho}_5''$, can be found via Jordan chain relations (see also Appendix D, for details). When found, the density matrix $\hat{\rho}(t)$ of the system can be decomposed in the form given in Eq. (15), with an additional contribution $c''_{\rm EP}(t)\hat{\rho}''_{\rm EP}$, where $\hat{\rho}''_{\rm EP}=\hat{\rho}_5''$ and $c''_{\rm EP}(t)=t^2\exp(\lambda_{\rm EP}t){\rm Tr}[\hat{\sigma}_5''\hat{\rho}(0)]$.

When $\kappa>\kappa^{\rm q}_{\rm LEP,1}$, one has to consider the symmetric $\hat{\rho}^{\rm s}_{3,4}$ and antisymmetric $\hat{\rho}^{\rm a}_{3,4}$ density matrices, as was explained above. Thus, one eventually finds the form of the eigenstates for the symmetric density matrices $\hat{\rho}^{\rm s}_{3,4}$:

$$\begin{aligned}
&|\psi_0^{(3,4)}\rangle_{\rm s}=|00\rangle,\quad |\psi_3^{(3,4)}\rangle_{\rm s}=|11\rangle,\\
&|\psi_{1,2}^{(3,4)}\rangle_{\rm s}\equiv-\delta|01\rangle+\Big(D^2\pm\sqrt{\delta^2+D^4}\Big)|10\rangle,
\end{aligned}\tag{55}$$

where $\delta=4\kappa A_-$. The antisymmetric matrices $\hat{\rho}^{\rm a}_{3,4}$, instead, have the following eigenstates

$$\begin{aligned}
&|\psi_0^{(3,4)}\rangle_{\rm a}=|00\rangle,\\
&|\psi_{1,2}^{(3,4)}\rangle_{\rm a}\equiv-4\kappa|01\rangle+\Big(A_-\pm\gamma\Big)|10\rangle,
\end{aligned}\tag{56}$$

where $\gamma=\sqrt{16\kappa^2+A_-^2}$. As one can see from Eqs. (55) and (56), the eigenstates of $\hat{\rho}_3^{\rm s,a}$ and $\hat{\rho}_4^{\rm s,a}$ are the same. This stems from the fact that $\hat{\rho}_4=\hat{\rho}_3^\dagger$ according to Eq. (50), in the case when $\kappa>\kappa^{\rm q}_{\rm LEP,1}$. As both Eqs. (55) and (56) infer, in this case, there is also no exact matching between the eigenstates of $\hat{H}_{\rm eff}$ and $\hat{\rho}^{\rm s,a}_{3,4}$ of the Liouvillian $\mathcal{L}$; thus, providing a different description of the

interaction between the cavities. In the limit $\kappa \to \infty$, the two antisymmetric intercavity eigenstates reduce to $|\psi^{(3,4)}_{1,2}\rangle_{\rm a} \equiv |10\rangle \pm |01\rangle$, whereas the symmetric intercavity eigenstates $|\psi^{(3,4)}_{2,3}\rangle$ reduce to either $|01\rangle$ or $|10\rangle$. According to Eqs. (10) and (48), away from the EPs, the elements $|\psi^{(3,4)}_n\rangle_{\rm s,a}\langle\psi^{(3,4)}_n|$ of the eigenmatrices $\hat{\rho}^{\rm s,a}_{3,4}$ in Eqs. (55) and (56), apart from the exponential decay, also acquire an oscillating term proportional to D.

(3) Study of $\hat{\rho}_{1,2,8,9}$.— Now let us focus on the non-Hermitian eigenmatrices $\hat{\rho}_i$, $i = 1,2,8,9$, given in Eq. (52). These eigenmatrices define the second LEP in the system:

$$\kappa^{\rm q}_{\rm LEP,2} = \frac{\left|(A+\Gamma_1)^2 - \Gamma_2^2\right|}{4\sqrt{A_+^2 - 8A\Gamma_2}}. \tag{57}$$

At the LEP $\kappa_{\rm LEP,2}$, one can observe the coalescence of the eigenmatrices $\hat{\rho}_1$ and $\hat{\rho}_2$, as well as the coalescence of the eigenmatrices $\hat{\rho}_8$ and $\hat{\rho}_9$, and the same applies to their Hermitian conjugate (see Fig. 6). Thus, the LEP $\kappa^{\rm q}_{\rm LEP,2}$ is of the *second order*. In particular, when $A \ll \Gamma_{1,2}$, which is true in the two-photon cutoff, the LEP $\kappa^{\rm q}_{\rm LEP,2}$ is also inclined to coincide with $\kappa^{\rm q}_{\rm LEP,1}$ and $\kappa^{\rm q}_{\rm HEP}$ (see Fig. 6). Importantly, the same conclusion, regarding the convergence of the LEPs to the HEP, remains valid even when we try to increase the gain A, i.e., by extending the Hilbert space to larger photon numbers (see Fig. 7).

By performing the eigen-decomposition of the Hermitian symmetric and antisymmetric eigenmatrices $\hat{\rho}^{\rm s,a}_i$, $i = 1,2,8,9$, the corresponding wave functions $|\psi^{(i)}_n\rangle$, in general, take the form of the following superpositions $|\psi^{(\rm s,a)}_n\rangle = \sum c_{ij}|i\rangle|j\rangle$. Moreover, away from the EPs, the eigenmatrices elements $|\psi^{(\rm s,a)}_n\rangle\langle\psi^{(\rm s,a)}_n|$, in addition to the gradual decay, rapidly oscillate around the cavity resonance frequency ω_c, according to Eqs. (10) and (48).

♣ *(4) Study of $\hat{\rho}_{5,6}$.*— The real eigenvalue $\lambda_{5,6}$ in Eq. (48) has both algebraic and geometric multiplicity of two. This means that there are two linearly independent eigenmatrices corresponding to this eigenvalue, and which are given in Eq. (51). The Hermitian non-diagonal eigenmatrix $\hat{\rho}_5$, along with the eigenstates $|00\rangle$ and $|11\rangle$, has the following intercavity maximally entangled states:

$$|\psi^{(5)}_{1,2}\rangle \equiv |01\rangle \pm |10\rangle. \tag{58}$$

On the other hand, the eigenmatrix $\hat{\rho}_6$ possesses only the following entangled states:

$$|\psi^{(6)}_{1,2}\rangle \equiv |01\rangle \pm i|10\rangle. \tag{59}$$

The elements $|\psi^{(j)}_n\rangle\langle\psi^{(j)}_n|$ of the eigenmatrix $\hat{\rho}_j$, $j = 5,6$, decay in time with the rate $\lambda_{5,6}$.

(5) Study of $\hat{\rho}_7$.— Finally, we find that the non-Hermitian eigenmatrices $\hat{\rho}_7$ and $\hat{\rho}_7^\dagger$ give the following intercavity eigenstates

$$|\psi^{(7)}_{1,2}\rangle \equiv |00\rangle \pm |11\rangle. \tag{60}$$

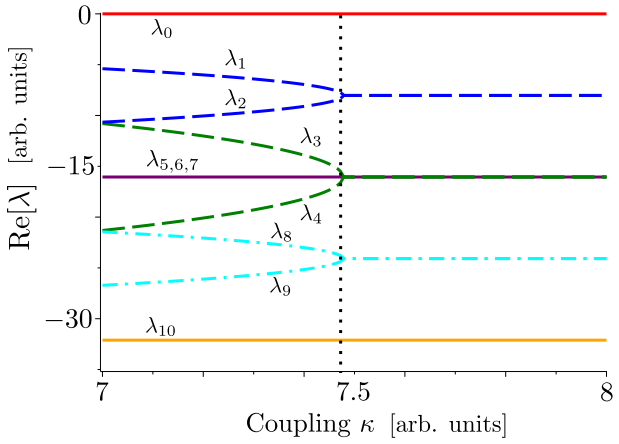

FIG. 6. Liouvillian EPs and the real part of its eigenvalues λ_j, according to Eq. (48): Re[λ_0] (red solid curve), Re[$\lambda_{1,2}$] (blue dash-dotted curves), Re[$\lambda_{3,4}$] (green dashed curves), Re[$\lambda_{5,6,7}$] (purple solid curve), Re[$\lambda_{8,9}$] (cyan dotted curves), and Re[λ_{10}] (orange solid curve). The gain in the active cavity $A = 0.01$ [arb. units], while the losses in the active and passive cavities are the same as in Fig. 2. The maximum value of the mean photon number in the active cavity is $\langle\hat{n}_1\rangle_{\rm max} \approx 3{\cdot}10^{-4}$. For comparison, the HEP (vertical grey dotted line) of the NHH, given in Eq. (45), is also displayed. This graph indicates that, in the single-photon regime, the LEPs and HEPs tend to coincide. Moreover, as it follows from the plot, the values of the two LEPs, given in Eqs. (53) and (57), also show the tendency to overlap.

The products $|\psi^{(7)}_{1,2}\rangle\langle\psi^{(7)}_{1,2}|$, which constitute the eigenmatrix $\hat{\rho}_7$, also decay with the same rate as the states $\hat{\rho}_{5,6}$, but oscillate at the double frequency $2\omega_c$, according to Eqs. (10) and (48).

(6) General discussion about the spectral decomposition.— In the single-photon limit, the LEPs and HEPs tend to coincide, as in the semiclassical case for many photons. On the other hand, the spectral properties of the Liouvillian drastically differ from those of the NHH and exhibit a rich dynamical nature.♣ Most importantly, even if the LEPs and HEPs coincide for the same set of the system parameters, they can have completely different order, thus, pointing to the different nature of HEPs and LEPs.

V. CONCLUSIONS

We have studied the quantum and semiclassical exceptional points of a linear non-Hermitian system of coupled cavities with losses and gain within the Scully-Lamb quantum laser model. Specifically, we have found the expressions for the HEPs and LEPs of the non-Hermitian system in both semiclassical and quantum regimes, i.e., when the system contains either classical fields with many photons or single photons, respectively. Our results have demonstrated that in either regime the position of both HEPs and LEPs tend to be the same. Moreover, phys-

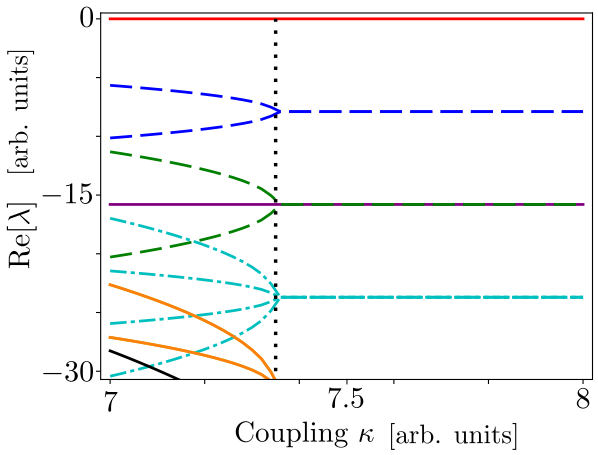

FIG. 7. Liouvillian EPs and the real part of its eigenvalues λ for a multiphoton system with up to eight photons in each cavity. The system parameters are: the gain in the active cavity $A = 0.5$ [arb. units], the losses in the active and passive cavities are the same as in Fig. 2. For comparison, the HEP of the NHH (vertical grey dotted line), given in Eq. (45), is also displayed. This graph indicates that with an increasing photon number in the system, the LEPs and HEP tend to coincide as in Fig. 6.

ical quantities such as the decay rates of the first order correlation functions are the same. In the semiclassical regime, we have calculated the HEP from the spectra of the effective non-Hermitian Hamiltonian, whereas the LEP has been determined from the two-time correlation function. Importantly, our analysis has also revealed that it is exactly a TTCF that enables to identify a true LEP in the semiclassical regime, whereas the field power spectra, in general, *fail* to reveal the exact value of the LEP. In the quantum mode, we have assumed that the system contains no more than one photon in each cavity; thus, allowing us to write down both the NHH and Liouvillian in a finite matrix form. Our calculations have also indicated that whereas the parameters for which HEPs and LEPs can coincide, the spectral structure of the Liouvillian is much richer compared to the NHH, revealing its full dynamical nature. ♣ Moreover, we have found that, in the quantum regime, the very order of EPs can be different for HEPs and LEPs, respectively, with LEPs being in general of higher order.

ACKNOWLEDGMENTS

The authors kindly acknowledge Alberto Biella, Nicola Bartolo, Şahin K. Özdemir, and Jan Peřina Jr. for insightful discussions. I.A. thanks the Grant Agency of the Czech Republic (Project No. 17-23005Y), the Project CZ.02.1.010.00.016_0190000754. F.M. is supported by the FY2018 JSPS Postdoctoral Fellowship for Research in Japan. F.N. is supported in part by the: MURI Center for Dynamic Magneto-Optics via the Air Force Office of Scientific Research (AFOSR) (FA9550-14-1-0040), Army Research Office (ARO) (Grant No. W911NF-18-1-0358), Asian Office of Aerospace Research and Development (AOARD) (Grant No. FA2386-18-1-4045), Japan Science and Technology Agency (JST) (via the Q-LEAP program, and the CREST Grant No. JPMJCR1676), Japan Society for the Promotion of Science (JSPS) (JSPS-RFBR Grant No. 17-52-50023, and JSPS-FWO Grant No. VS.059.18N), and the RIKEN-AIST Challenge Research Fund.

APPENDICES

Appendix A: Some remarks regarding the use of quantum Langevin forces in Sec. IIIA

Here, we would like to make a few comments regarding the widespread use of quantum Langevin forces, given in Eq. (31), and which encompass the quantum noise in the system.

In the usual approach, applied in the related literature [71, 72], especially devoted to the $\mathcal{PT}$-symmetric cavities, one may encounter the following Langevin equations for the quantum fields $\hat{a}_1$ and $\hat{a}_2$ in the coupled cavities (ignoring the complex frequency part):

$$\begin{aligned}\frac{\mathrm{d}}{\mathrm{d}t}\hat{a}_1 &= \frac{g_1}{2}\hat{a}_1 - \kappa\hat{a}_2 + \sqrt{g_1}\hat{f}_1^\dagger,\\ \frac{\mathrm{d}}{\mathrm{d}t}\hat{a}_2 &= -\frac{g_2}{2}\hat{a}_2 + \kappa\hat{a}_1 + \sqrt{g_2}\hat{l}_2,\end{aligned} \tag{A1}$$

where $g_1 > 0$ ($g_2 > 0$) describes amplification (damping) in the active (passive) cavity, and $\hat{f}_j^\dagger$ ($\hat{l}_j$) is the quantum Langevin force describing quantum noise amplification (dissipation) in the jth cavity. Moreover, one applies the Markovian approximation, i.e.,

$$[\hat{O}_j(t), \hat{O}_k^\dagger(t')] = \delta_{jk}\delta(t-t'), \tag{A2}$$

where $\hat{O} = \hat{f}$, and $\hat{l}, j = 1, 2$.

In the case when there are no thermal photons in the environment, one obtains

$$\langle \hat{f}_j(t)\hat{f}_j^\dagger(t')\rangle = \langle \hat{l}_j(t)\hat{l}_j^\dagger(t')\rangle = \delta(t-t'). \tag{A3}$$

For the case when $\kappa = 0$, by direct calculation using Eq. (A1), one acquires the following expression for the mean photon number in the active cavity:

$$\langle \hat{n}_1(t)\rangle = \exp(2g_1 t) - 1. \tag{A4}$$

Needless to say, the last expression diverges in the limit $t \to \infty$. In this case, one needs to incorporate a nonlinear term in the first equation in Eq. (A1) accountable for gain saturation.

For the case when the active cavity is below the lasing threshold, and again assuming $\kappa = 0$, by blindly replacing the gain g_1 in Eq. (A1) by the net negative gain

$g_1 = A - \Gamma_1 < 0$, where A is the total gain, and Γ_1 is the total loss in the active cavity, one obtains the unphysical solution with $\langle \hat{n}_1(t) \rangle < 0$. To resolve the latter problem, one has to modify Eq. (A1) with an additional noise operator $\hat{l}_1$ responsible for dissipation, i.e.,

$$\begin{aligned} \frac{\mathrm{d}}{\mathrm{d}t}\hat{a}_1 &= \frac{A-\Gamma_1}{2}\hat{a}_1 - \kappa\hat{a}_2 + \sqrt{A}\hat{f}_1^\dagger + \sqrt{\Gamma_1}\hat{l}_1, \\ \frac{\mathrm{d}}{\mathrm{d}t}\hat{a}_2 &= -\frac{\Gamma_2}{2}\hat{a}_2 + \kappa\hat{a}_1 + \sqrt{\Gamma_2}\hat{l}_2. \end{aligned} \tag{A5}$$

Now, the rate equations in the form given in Eq. (A5) provide the same spectral properties of the system as the rate equations derived from the linear Scully-Lamb ME in Eq. (7).

It is important to stress that even the Langevin equations in Eq. (31) for the effective NHH $\hat{H}_{\rm eff}$, given in Eq. (8), may lead to erroneous results when the laser cavity operates near the threshold. In this case, it is a necessity to apply the general Scully-Lamb ME in Eq. (2) [38].

Appendix B: Some additional calculations provided for Sec. IIIB

1. Coefficients for the TTCFs in Eq. (36)

The coefficients $u_{1,2}$ and $v_{1,2}$ in Eq. (36) have the following forms:

$$\begin{aligned} u_{1,2} =& \frac{-A}{2N}\Big[\Big(\Gamma_2(A-\Gamma_+) - 4\kappa^2\Big)\beta \\ & \pm (A-\Gamma_+)\Big(\Gamma_2(A-\Gamma_-) - 4\kappa^2\Big)\Big], \\ v_{1,2} =& \frac{2A\kappa^2}{N}\Big[\beta \pm (A-\Gamma_+)\Big], \end{aligned} \tag{B1}$$

where

$$N = (A-\Gamma_+)\Big[(A-\Gamma_1)\Gamma_2 - 4\kappa^2\Big]\beta. \tag{B2}$$

2. Formulas for constants P_i and Q_i in Eq. (38)

For the TTCFs $\langle \hat{a}_i^\dagger(0)\hat{a}_i(\tau)\rangle_{\rm ss}$, $i = 1, 2$, the expressions for P_i and Q_i become

$$\begin{aligned} P_1 &= -A\frac{4\Gamma_2^2 + (A-\Gamma_+)^2}{(A-\Gamma_+)^3}, \\ Q_1 &= -A\frac{(A-\Gamma_+)(A-\Gamma_-)(A-\Gamma_1-3\Gamma_2)}{4(A-\Gamma_+)^3}, \\ P_2 &= -A\frac{(A-\Gamma_-)^2}{(A-\Gamma_+)^3}, \\ Q_2 &= A\frac{(A-\Gamma_-)^2}{4(A-\Gamma_+)^2}. \end{aligned} \tag{B3}$$

For the linear system under consideration, the following condition $(A-\Gamma_+ < 0)$ is always satisfied. The latter implies that the constants $P_{1,2}$ and Q_2 are always positive-valued. On the other hand, the positivity (negativity) of the constant Q_1 is determined by the positivity (negativity) of the expression $A - \Gamma_-$, which can be either positive or negative.

3. Resonant frequencies of the power spectra S_1 and S_2 presented in Fig. 5.

The frequencies of the resonant peaks in the emission spectra $S_j(\omega)$ can be found as the maxima of the functions $S_1(\omega)$ and $S_2(\omega)$. By solving the equations

$$\frac{\mathrm{d}S_j(\omega)}{\mathrm{d}\omega} = 0, \quad j = 1, 2,$$

with respect to ω one finds the following relations for the spectral peaks in both cavities:

$$\begin{aligned} \omega_1^\pm &= \omega_c \pm \frac{1}{2}\mathrm{Re}\left[\left(2\kappa\sqrt{4\kappa^2 + 2\Gamma_2(\Gamma_2 - G_1)} - \Gamma_2^2\right)^{\frac{1}{2}}\right], \\ \omega_2^\pm &= \omega_c \pm \frac{1}{4}\mathrm{Re}\left[\sqrt{16\kappa^2 - 2(G_1^2 + \Gamma_2^2)}\right]. \end{aligned} \tag{B4}$$

From Eq. (B4), one can easily find the conditions at which the two resonant peaks coalesce in either cavity, as given in Eq. (41).

Appendix C: Liouvillian eigenmatrices $\hat{\rho}_i$ given in Eqs. (49)–(52)

Within the effective Hilbert space spanned by the vectors $|jk\rangle$, $j, k = 0, 1$, the annihilation boson operators for the fields $\hat{a}_1$ and $\hat{a}_2$ in the active and passive cavities take the following matrix forms

$$\hat{a}_1 = \begin{pmatrix} 0 & 1 \\ 0 & 0 \end{pmatrix} \otimes \hat{I}, \quad \hat{a}_2 = \hat{I} \otimes \begin{pmatrix} 0 & 1 \\ 0 & 0 \end{pmatrix}, \tag{C1}$$

respectively, where $\hat{I}$ is the 2×2 identity matrix. By using the matrix representation of the boson operators in Eq. (C1), one can straightforwardly calculate the eigenvalues and eigenmatrices of the Liouvillian $\mathcal{L}$ in Eqs. (7) and (9). Below, we write the elements of the Liouvillian eigenmatrices $\hat{\rho}_j$ given in Eqs. (49)–(52).

1. Liouvillian eigenmatrix $\hat{\rho}_0$ in Eq. (49)

The elements of the steady-state eigenmatrix $\hat{\rho}_0$, given in Eq. (49), are

$$\begin{aligned} \rho_{00} &= \Gamma_1\Gamma_2 A_+^2 + 4\kappa^2\Gamma_+^2, \\ \rho_{01} &= 4A\kappa^2\Gamma_+, \\ \rho_{10} &= A\left(\Gamma_2 A_+^2 + 4\kappa^2\Gamma_+\right), \\ \rho_{11} &= 4A\kappa^2, \\ N_0 &= A_+^2\Big(4\kappa^2 + \Gamma_2(A+\Gamma_1)\Big). \end{aligned} \tag{C2}$$

2. Liouvillian eigenmatrix $\hat{\rho}_{10}$ in Eq. (49)

The elements of the traceless eigenmatrix $\hat{\rho}_{10}$, in Eq. (49), become

$$\hat{\rho}_{10} = \mathrm{diag}(1,-1,-1,1). \tag{C3}$$

3. Liouvillian eigenmatrices $\hat{\rho}_{3,4}$ in Eq. (50)

The elements of the traceless eigenmatrices $\hat{\rho}_{3,4}$, given in Eq. (50), take the form

$$\begin{aligned}
\rho'_{00} \pm f_1 D &= -8\kappa^2\Gamma_- - \Gamma_2 A_-^2 \pm \Gamma_2 A_- D,\\
\rho'_{01} \pm f_2 D &= -4\kappa^2(A-\Gamma_+) \pm 4\kappa^2 D,\\
\rho'_{0110} \pm f_3 D &= -2\kappa(\Gamma_2 A_- + 8\kappa^2) \pm 2\kappa\Gamma_2 D,\\
\rho'_{10} \pm f_4 D &= \Gamma_2 A_-^2 - 4\kappa^2(A-\Gamma_1+3\Gamma_2)\\
&\quad \pm(\Gamma_2^2 - \Gamma_2(A+\Gamma_1) + 4\kappa^2)D,\\
\rho_{11} &= 8A\kappa^2.
\end{aligned} \tag{C4}$$

4. Liouvillian eigenmatrix $\hat{\rho}_5$ in Eq. (51)

The elements of the traceless Hermitian eigenmatrix $\hat{\rho}_5$, given in Eq. (51), are written as follows

$$\begin{aligned}
&\rho_{00} = -8\Gamma_+\kappa^2, \quad \rho_{01} = \rho_{10} = -4\kappa^2(A-\Gamma_+),\\
&\rho_{0110} = -\kappa\Big[4A\Gamma_1 + (A-\Gamma_+)(A-\Gamma_-)\Big], \quad \rho_{11} = 8A\kappa^2.
\end{aligned} \tag{C5}$$

5. Liouvillian eigenmatrices $\hat{\rho}_{1,2,8,9}$ in Eq. (52)

The elements of the traceless eigenmatrices $\hat{\rho}_{1,2,8,9}$, given in Eq. (52), have the following forms:

$$\begin{aligned}
\rho_{0001} &= 4\kappa\left[\pm E_\pm(\Gamma_+ - A) \pm F + A_+^2 - 4A\Gamma_2\right],\\
\rho_{0010} &= \pm E_\pm\left(\Gamma_2^2 - (A+\Gamma_1)^2 \pm F\right) \pm 2\Gamma_2 F\\
&\quad +2\Gamma_2(\Gamma_2^2 - (A+\Gamma_1)^2) + 16\kappa^2(A-\Gamma_+),\\
\rho_{0111} &= 32A\kappa^2,\\
\rho_{1011} &= 8A\kappa(2\Gamma_2 \pm E_\pm),
\end{aligned} \tag{C6}$$

where $E_\pm$ and F are given in Eq. (48).

The eigenmatrices $\hat{\rho}_{1,2}$ have the elements given in Eq. (C6) with $E_\pm$ and $\pm F$, respectively. The eigenmatrices $\hat{\rho}_{8,9}$ have the elements given in Eq. (C6) with $-E_\pm$ and $\pm F$, respectively.

Appendix D: Hermitian pseudo-eigenmatrices $\hat{\rho}'_5$ and $\hat{\rho}''_5$

The generalized pseudo-eigenmatrices $\hat{\rho}'_5$ and $\hat{\rho}''_5$ can be found from the eigenmatrix $\hat{\rho}_5$, given in Eq. (51), by applying Jordan chain relations, i.e.,

$$\begin{aligned}
\mathcal{L}\hat{\rho}_5 - \lambda_{\mathrm{LEP}}\hat{\rho}_5 &= 0,\\
\mathcal{L}\hat{\rho}'_5 - \lambda_{\mathrm{LEP}}\hat{\rho}'_5 &= \hat{\rho}_5,\\
\mathcal{L}\hat{\rho}''_5 - \lambda_{\mathrm{LEP}}\hat{\rho}''_5 &= \hat{\rho}'_5.
\end{aligned} \tag{D1}$$

By combining together Eqs. (51) and (D1), one can straightforwardly arrive at the pseudo-eigenmatrices $\hat{\rho}'_5$ and $\hat{\rho}''_5$, which have the following general form:

$$\hat{\rho}_5^j \equiv \begin{pmatrix} a^j & 0 & 0 & 0\\ 0 & b^j & \alpha^j & 0\\ 0 & \alpha^j & c^j & 0\\ 0 & 0 & 0 & d^j \end{pmatrix}, \quad j = \{',''\}. \tag{D2}$$

The elements of the pseudo-eigenmatrix $\hat{\rho}'_5$ have the following form:

$$\begin{aligned}
a' &= 2\Gamma_2 A_- - 2\Gamma_+, \quad b' = \tfrac{1}{2}A_-^2 - (A-\Gamma_+),\\
c' &= -\tfrac{1}{2}A_+^2 + 2\Gamma_2^2 - (A-\Gamma_+), \quad d' = 2A,\\
\alpha' &= \Gamma_2 A_- - A_+.
\end{aligned} \tag{D3}$$

And the elements of the pseudo-eigenmatrix $\hat{\rho}''_5$ read as follows

$$\begin{aligned}
a'' &= \tfrac{6\Gamma_2{}^2 + (-6A - 4\Gamma_1 + 8)\Gamma_2 - 2\Gamma_1(A+\Gamma_1)}{A_-},\\
c'' &= \tfrac{-5\Gamma_2{}^2 + (6A + 4\Gamma_1 - 6)\Gamma_2 - A^2 + \Gamma_1{}^2 - 2A - 2\Gamma_1}{A_-},\\
b'' &= 2 - (A-\Gamma_+), \quad d'' = 2A, \quad \alpha'' = -\tfrac{-2\Gamma_2(A_- - 2)}{A_-}.
\end{aligned} \tag{D4}$$

It is assumed that all elements of the pseudo-eigenmatrices $\hat{\rho}'_5$ and $\hat{\rho}''_5$, given in Eqs. (D3) and (D4), respectively, have the same dimensionality.

The eigenstates of these Hermitian pseudo-eigenmatrices, which describe the intercavity interaction, become of the form:

$$|\psi_5^j\rangle_\pm \equiv 2\alpha^j|10\rangle + \left(c^j - b^j \pm \sqrt{4(\alpha^j)^2 + (b^j - c^j)^2}\right)|01\rangle, \tag{D5}$$

with $j = \{',''\}$, and where α^j, b^j, and c^j are given in Eqs. (D3) and (D4).

[1] C. M. Bender and S. Boettcher, "Real spectra in non-Hermitian Hamiltonians having $\mathcal{PT}$ symmetry," Phys. Rev. Lett. **80**, 5243–5246 (1998).

[2] Ş. K. Özdemir, S. Rotter, F. Nori, and L. Yang, "Parity-time symmetry and exceptional points in photonics," Nature Materials **18**, 783 (2019).

[3] M. Miri and A. Alù, "Exceptional points in optics and photonics," Science **363**, 7709 (2019).

[4] L. Feng, R. El-Ganainy, and L. Ge, "Non-Hermitian photonics based on parity-time symmetry," Nat. Photon. **11**, 752 (2017).

[5] R. El-Ganainy, K. G. Makris, M. Khajavikhan, Z. H. Musslimani, S. Rotter, and D. N. Christodoulides, "Non-Hermitian physics and $\mathcal{PT}$ symmetry," Nat. Phys. **14**, 11 (2018).

[6] D. Christodoulides and J. Yang, eds., *Parity-time Symmetry and Its Applications* (Springer Singapore, 2018).

[7] Z. Lin, H. Ramezani, T. Eichelkraut, T. Kottos, H. Cao, and D. N. Christodoulides, "Unidirectional invisibility induced by $\mathcal{PT}$-symmetric periodic structures," Phys. Rev. Lett. **106**, 213901 (2011).

[8] A. Regensburger, C. Bersch, M.-A. Miri, G. Onishchukov, D. N. Christodoulides, and U. Peschel, "Parity-time synthetic photonic lattices," Nature (London) **488**, 167 (2012).

[9] L. Feng, Z. J. Wong, R.-M. Ma, Y. Wang, and X. Zhang, "Single-mode laser by parity-time symmetry breaking," Science **346**, 972 (2014).

[10] H. Hodaei, M.-A. Miri, M. Heinrich, D. N. Christodoulides, and M. Khajavikhan, "Parity-time-symmetric microring lasers," Science **346**, 975 (2014).

[11] B. Peng, Ş. K. Özdemir, F. Lei, F. Monifi, M. Gianfreda, G. L. Long, S. Fan, F. Nori, C. Bender, and L. Yang, "Parity-time-symmetric whispering-gallery microcavities," Nat. Phys. **10**, 394 (2014).

[12] L. Chang, X. Jiang, S. Hua, C. Yang, J. Wen, L. Jiang, G. Li, G. Wang, and M. Xiao, "Parity-time symmetry and variable optical isolation in active-passive-coupled microresonators," Nat. Photon. **8**, 524 (2014).

[13] H. Jing, Ş. K. Özdemir, X.-Y. Lü, J. Zhang, L. Yang, and F. Nori, "$\mathcal{PT}$-symmetric phonon laser," Phys. Rev. Lett. **113**, 053604 (2014).

[14] H. Lü, Ş. K. Özdemir, L. M. Kuang, F. Nori, and H. Jing, "Exceptional points in random-defect phonon lasers," Phys. Rev. App. **8**, 044020 (2017).

[15] Z.-P. Liu, J. Zhang, Ş. K. Özdemir, B. Peng, H. Jing, X.-Y. Lü, C.-W. Li, L. Yang, F. Nori, and Y.-X. Liu, "Metrology with $\mathcal{PT}$-symmetric cavities: Enhanced sensitivity near the $\mathcal{PT}$-phase transition," Phys. Rev. Lett. **117**, 110802 (2016).

[16] W. Chen, Ş. K. Özdemir, G. Zhao, J. Wiersig, and L. Yang, "Exceptional points enhance sensing in an optical microcavity," Nature (London) **548**, 192 (2017).

[17] H. Hodaei, U. H. Absar, S. Wittek, H. Garcia-Gracia, R. El-Ganainy, D. N. Christodoulides, and M. Khajavikhan, "Enhanced sensitivity at higher-order exceptional points," Nature (London) **548**, 187 (2017).

[18] M. Brandstetter, M. Liertzer, C. Deutsch, P. Klang, J. Schoberl, H. E. Tureci, G. Strasser, K. Unterrainer, and S. Rotter, "Reversing the pump dependence of a laser at an exceptional point," Nat. Commun. **5**, 4034 (2014).

[19] B. Peng, Ş. K. Özdemir, S. Rotter, H. Yilmaz, M. Liertzer, F. Monifi, C. M. Bender, F. Nori, and L. Yang, "Loss-induced suppression and revival of lasing," Science **346**, 328 (2014).

[20] J. Schindler, A. Li, M.C. Zheng, F. M. Ellis, and T. Kottos, "Experimental study of active LRC circuits with $\mathcal{PT}$ symmetries," Phys. Rev. A **84**, 040101(R) (2011).

[21] H. Xu, D. Mason, L. Jiang, and J. G. E. Harris, "Topological energy transfer in an optomechanical system with exceptional points," Nature (London) **537**, 80 (2016).

[22] H. Jing, Ş. K. Özdemir, H. Lü, and F. Nori, "High-order exceptional points in optomechanics," Scientific Reports **7**, 3386 (2017).

[23] X. Zhu, H. Ramezani, C. Shi, J. Zhu, and X. Zhang, "$\mathcal{PT}$-symmetric acoustics," Phys. Rev. X **4**, 031042 (2014).

[24] R. Fleury, D. Sounas, and A. Alù, "An invisible acoustic sensor based on parity-time symmetry," Nat. Commun. **6**, 5905 (2015).

[25] H. Benisty, A. Degiron, A. Lupu, A. De Lustrac, S. Chenais, S. Forget, M. Besbes, G. Barbillon, A. Bruyant, S. Blaize, and G. Lerondel, "Implementation of $\mathcal{PT}$ symmetric devices using plasmonics: principle and applications," Optics Express **19**, 18004 (2011).

[26] M. Kang, F. Liu, and J. Li, "Effective spontaneous $\mathcal{PT}$-symmetry breaking in hybridized metamaterials," Phys. Rev. A **87**, 053824 (2013).

[27] D. Leykam, K. Y. Bliokh, C. Huang, Y. D. Chong, and F. Nori, "Edge modes, degeneracies, and topological numbers in non-hermitian systems," Phys. Rev. Lett. **118**, 040401 (2017).

[28] J. González and R. A. Molina, "Topological protection from exceptional points in weyl and nodal-line semimetals," Phys. Rev. B **96**, 045437 (2017).

[29] W. Hu, H. Wang, P. Ping Shum, and Y. D. Chong, "Exceptional points in a non-hermitian topological pump," Phys. Rev. B **95**, 184306 (2017).

[30] T. Gao, G. Li, E. Estrecho, T. C. H. Liew, D. Comber-Todd, A. Nalitov, M. Steger, K. West, L. Pfeiffer, D. W. Snoke, A. V. Kavokin, A. G. Truscott, and E. A. Ostrovskaya, "Chiral modes at exceptional points in exciton-polariton quantum fluids," Phys. Rev. Lett. **120**, 065301 (2018).

[31] T. Liu, Y.-R. Zhang, Q. Ai, Z. Gong, K. Kawabata, M. Ueda, and F. Nori, "Second-order topological phases in non-Hermitian systems," Phys. Rev. Lett. **122**, 076801 (2019).

[32] L. Zhou, Q.-h. Wang, H. Wang, and J. Gong, "Dynamical quantum phase transitions in non-hermitian lattices," Phys. Rev. A **98**, 022129 (2018).

[33] K. Y. Bliokh, D.l Leykam, M. Lein, and F. Nori, "Topological non-Hermitian origin of surface Maxwell waves," Nature Communications **10**, 580 (2019).

[34] M. van Caspel, S. E. T. Arze, and I. P. Castillo, "Dynamical signatures of topological order in the driven-dissipative Kitaev chain," SciPost Phys. **6**, 26 (2019).

[35] Z.-Y. Ge, Y.-R. Zhang, T. Liu, S.-W. Li, H. Fan, and F. Nori, "Topological band theory for non-hermitian systems from the Dirac equation," Phys. Rev. B **100**, 054105 (2019).

[36] T. Yoshida, R. Peters, N. Kawakami, and Y. Hatsugai, "Symmetry-protected exceptional rings in two-dimensional correlated systems with chiral symmetry," Phys. Rev. B **99**, 121101 (2019).

[37] S. Scheel and A. Szameit, "$\mathcal{PT}$-symmetric photonic quantum systems with gain and loss do not exist," EPL

122, 34001 (2018).
[38] M. Sargent III, M. Scully, and W. Lamb Jr., *Laser Physics* (Westview Press, Boulder, CO, 1974).
[39] G. Agarwal, *Quantum Optics* (Cambridge University Press, Cambridge, UK, 2013).
[40] S. Haroche and J. M. Raimond, *Exploring the Quantum: Atoms, Cavities, and Photons* (Oxford University Press, Oxford, 2006).
[41] J. Gea-Banacloche, "Emergence of classical radiation fields through decoherence in the Scully-Lamb laser model," Found. Phys. **28**, 531 (1997).
[42] Zh.-Y. Zhou, Y.-A. Yan, S. Hughes, J. Q. You, and F. Nori, "Accessing the bath information in open quantum systems with the stochastic c-number Langevin equation method," (2019), arXiv:1905.11119.
[43] F. Minganti, A. Miranowicz, R. W. Chhajlany, and F. Nori, "Quantum exceptional points of non-Hermitian Hamiltonians and Liouvillians: The effects of quantum jumps," (2019), arxiv:1909.11619.
[44] T. Prosen, "$\mathbb{PT}$-symmetric quantum liouvillean dynamics," Phys. Rev. Lett. **109**, 090404 (2012).
[45] F. Minganti, A. Biella, N. Bartolo, and C. Ciuti, "Spectral theory of Liouvillians for dissipative phase transitions," Phys. Rev. A **98**, 042118 (2018).
[46] K. Macieszczak, M. Guţă, I. Lesanovsky, and J. P. Garrahan, "Towards a theory of metastability in open quantum dynamics," Phys. Rev. Lett. **116**, 240404 (2016).
[47] N. Hatano, "Exceptional points of the Lindblad operator of a two-level system," Molecular Physics **117**, 2121 (2019).
[48] V. V. Albert and L. Jiang, "Symmetries and conserved quantities in Lindblad master equations," Phys. Rev. A **89**, 022118 (2014).
[49] M. S. Sarandy and D. A. Lidar, "Adiabatic approximation in open quantum systems," Phys. Rev. A **71**, 012331 (2005).
[50] T. Prosen, "Spectral theorem for the Lindblad equation for quandratic open fermionic systems," Journal of Statistical Mechanics: Theory and Experiment **2010**, P07020 (2010).
[51] Y. Yamamoto and A. Imamoğlu, *Mesoscopic Quantum Optics* (John Wiley and Sons, New York, 1999).
[52] A. J. Hoffman, S. J. Srinivasan, S. Schmidt, L. Spietz, J. Aumentado, H. E. Türeci, and A. A. Houck, "Dispersive photon blockade in a superconducting circuit," Phys. Rev. Lett. **107**, 053602 (2011).
[53] J. Lebreuilly, A. Biella, F. Storme, D. Rossini, R. Fazio, C. Ciuti, and I. Carusotto, "Stabilizing strongly correlated photon fluids with non-Markovian reservoirs," Phys. Rev. A **96**, 033828 (2017).
[54] J. Lebreuilly, M. Wouters, and I. Carusotto, "Towards strongly correlated photons in arrays of dissipative nonlinear cavities under a frequency-dependent incoherent pumping," Comptes Rendus Physique **17**, 836 – 860 (2016), polariton physics / Physique des polaritons.
[55] A. Biella, F. Storme, J. Lebreuilly, D. Rossini, R. Fazio, I. Carusotto, and C. Ciuti, "Phase diagram of incoherently driven strongly correlated photonic lattices," Phys. Rev. A **96**, 023839 (2017).
[56] O. Scarlatella, R. Fazio, and M. Schiró, "Emergent finite frequency criticality of driven-dissipative correlated lattice bosons," Phys. Rev. B **99**, 064511 (2019).
[57] T. Fink, A. Schade, S. Höfling, C. Schneider, and A. Imamoglu, "Signatures of a dissipative phase transition in photon correlation measurements," Nature Physics **14**, 365–369 (2018).
[58] D. F. Walls and G. J. Milburn, *Quantum Optics* (Springer, Berlin, 2011).
[59] K. Hashimoto, K. Kanki, H. Hayakawa, and T. Petrosky, "Non-divergent representation of a non-Hermitian operator near the exceptional point with application to a quantum Lorentz gas," Prog. Theor. Exp. Phys. **023A02**, 1 (2015).
[60] K. Kanki, S. Garmon, S. Tanaka, and T. Petrosky, "Exact description of coalescing eigenstates in open quantum systems in terms of microscopic Hamiltonian dynamics," J. Math. Phys. **58**, 092101 (2017).
[61] C. W. Gardiner and P. Zoller, *Quantum Noise* (Springer-Verlag, Berlin, 2000).
[62] F. Haake, "Density operator and multitime correlation functions for open systems," Phys. Rev. A **3**, 1723–1734 (1971).
[63] H. J. Carmichael, *Statistical Methods in Quantum Optics 1* (Springer, Berlin, 2010).
[64] I. I. Arkhipov, A. Miranowicz, O. Di Stefano, R. Stassi, S. Savasta, F. Nori, and Ş. K. Özdemir, "Scully-Lamb quantum laser model for parity-time-symmetric whispering-gallery microcavities: Gain saturation effects and nonreciprocity," Phys. Rev. A **99**, 053806 (2019).
[65] B. D. Hauer, J. Maciejko, and J. P. Davis, "Nonlinear power spectral densities for the harmonic oscillator," Ann. of Phys. **361**, 148 (2015).
[66] G. Yoo, H.-S. Sim, and H. Schomerus, "Quantum noise and mode nonorthogonality in non-Hermitian $\mathcal{PT}$-symmetric optical resonators," Phys. Rev. A **84**, 063833 (2011).
[67] H. Schomerus, "Quantum noise and self-sustained radiation of $\mathcal{PT}$-symmetric systems," Phys. Rev. Lett. **104**, 233601 (2010).
[68] Z. Cai and T. Barthel, "Algebraic versus exponential decoherence in dissipative many-particle systems," Phys. Rev. Lett. **111**, 150403 (2013).
[69] D. Poletti, P. Barmettler, A. Georges, and C. Kollath, "Emergence of glasslike dynamics for dissipative and strongly interacting bosons," Phys. Rev. Lett. **111**, 195301 (2013).
[70] R. Bouganne, M. B. Aguilera, A. Ghermaoui, J. Beugnon, and F. Gerbier, "Anomalous decay of coherence in a dissipative many-body system," Nat. Phys. (2019), 10.1038/s41567-019-0678-2.
[71] K. V. Kepesidis, T. J.. Milburn, J. Huber, K. G.. Makris, S. Rotter, and P. Rabl, "$\mathcal{PT}$-symmetry breaking in the steady state of microscopic gain–loss systems," New J. Phys. **18**, 095003 (2016).
[72] S. Vashahri-Ghamsari, B. He, and M. Xiao, "Continuous-variable entanglement generation using a hybrid $\mathcal{PT}$-symmetric system," Phys. Rev. A **96**, 033806 (2017).